JCI insight

Photoinactivation of catalase sensitizes wide-ranging bacteria to ROS-producing agents and immune cells

Pu-Ting Dong, … , George Y. Liu, Ji-Xin Cheng

JCI Insight. 2022. https://doi.org/10.1172/jci.insight.153079.

Research In-Press Preview Infectious disease Microbiology

Graphical abstract

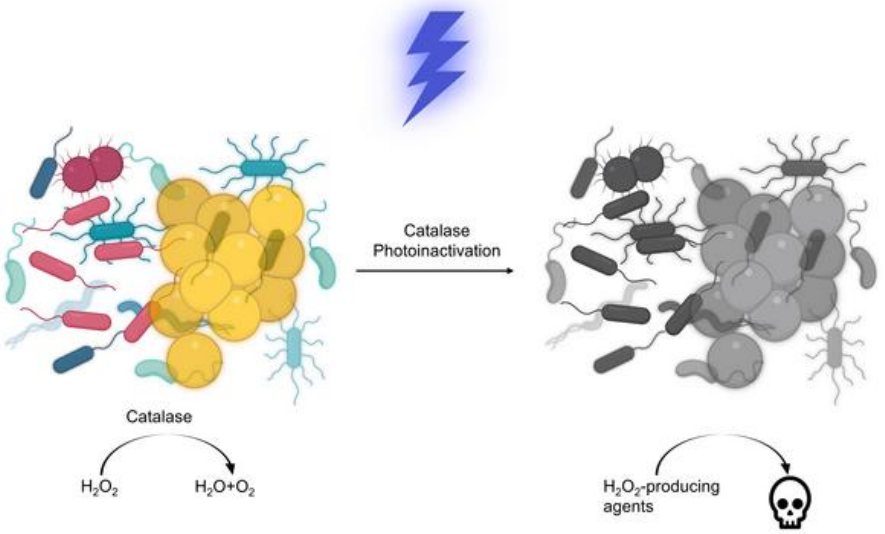

Photoinactivation of Catalase Sensitizes Wide-Ranging Bacteria to ROS-Producing Agents and Immune Cells

Pu-Ting Dong[1,2,#], Sebastian Jusuf[1,2,#], Jie Hui[1,2,#], Yuewei Zhan[1,2,#], Yifan Zhu[2,3], George Y. Liu[4,5], Ji-Xin Cheng[1,2,3,*]

[1]Department of Biomedical Engineering, Boston University, Boston, MA02215, USA.

[2]Photonics Center, Boston University, Boston, MA02215, USA.

[3]Department of Chemistry, Boston University, Boston, MA02215, USA.

[4]Division of Pediatric Infectious Diseases and Research Division of Immunology, Department of Biomedical Sciences, Cedars-Sinai Medical Center, Los Angeles, California, CA90048, USA.

[5]Division of Infectious Diseases, Department of Pediatrics, UCSD, San Diego, California, CA92093, USA.

Corresponding author: Dr. Ji-Xin Cheng, 8 St Mary's Street, Boston, MA02215.

Email: jxcheng@bu.edu; Phone: (617)-353-1276.

[#]These authors contributed equally: Pu-Ting Dong, Sebastian Jusuf, Jie Hui, Yuewei Zhan.

Abstract

Bacteria have evolved to cope with the detrimental effects of reactive oxygen species (ROS) using their essential molecular components. Catalase, a heme-containing tetramer protein expressed universally in most of the aerobic bacteria, plays an indispensable role in scavenging excess hydrogen peroxide (H_2O_2). Here, through utilization of wild-type and catalase-deficient mutants, we identified catalase as an endogenous therapeutic target of 400-420 nm blue light. Catalase residing inside bacteria could be effectively inactivated by blue light, subsequently rendering the pathogens extremely vulnerable to H_2O_2 and H_2O_2-producing agents. As a result, photoinactivation of catalase and H_2O_2 synergistically eliminate a wide range of catalase-positive planktonic bacteria and *P. aeruginosa* inside biofilms. In addition, photoinactivation of catalase is shown to facilitate macrophages to defend against intracellular pathogens. The antimicrobial efficacy of catalase photoinactivation is further validated using a *Pseudomonas aeruginosa*-induced mice abrasion model. Taken together, our findings offer a catalase-targeting phototherapy approach against multidrug-resistant bacterial infections.

Introduction

Antibiotic resistance remains one of the biggest threats to global health over the past decades. In United States alone, it is estimated that at least 2.8 million people are infected by antibiotic-resistant bacterial infections annually (1). Despite these alarming numbers, the pace of antibiotic resistance development is faster than that of clinical introduction of new antibiotics (2). If no efforts are made to curtail this situation, life loss from antibiotic-resistant infections might surpass cancer, and 10 million people will be killed worldwide by 2050 (3). Moreover, the imprudent use of antibiotics from clinical over-prescription and food industry escalates the selection of multi-drug resistant or even pan-drug resistant bacteria (4).

Confronted with this dire situation, antimicrobial blue light has emerged as a novel approach to combat multidrug-resistant bacterial infections (5, 6). Blue light in the 405-420 nm or the 450-470 nm optical windows has demonstrated bactericidal effects towards a wide range of microbial species, including gram-positive bacteria, gram-negative bacteria, mycobacteria, and molds (6). Of note, blue light has been utilized for clinical treatment of *Propionibacterium acnes* (7). *Helicobacter pylori*, the major cause of peptic ulcer disease, could be efficiently inactivated *in vitro* by visible light (8, 9). Besides planktonic-form bacteria, blue light also decreased the viability of *Pseudomonas aeruginosa* (*P. aeruginosa*), MRSA USA300 and *Candida albicans* in biofilm conditions (10). Importantly, no evidence of blue light-resistance development by pathogens has been documented after consecutive blue light treatments (11-13). Blue light has also been allied with other antimicrobial agents to eradicate bacteria. For example, quinine in combination with blue light exposure has shown efficacy to eliminate gram-negative *P. aeruginosa*, *Acinetobacter baumannii* (*A. baumannii*) (5) and *Candida albicans* (14). Blue light irradiance was also reported to enhance the inactivation efficacy of low-concentration chlorinated disinfectants towards *Clostridium difficile* (15). Blue light (460 nm) plus hydrogen peroxide (H_2O_2) exhibited high efficacy to eradicate MRSA by devastating its functional membrane domain (16, 17).

Despite these advances, the working mechanism of antimicrobial blue light has remained elusive for years. Endogenous metal-free porphyrin or riboflavin has been considered as the major molecular targets (6). It is assumed that reactive oxygen species (ROS) produced from photodynamic reaction between blue light and these endogenous chromophores lead to bacterial death. However, this hypothesis has remained controversial. The concentration of endogenous porphyrins or riboflavin is as low as $2\text{-}4\times10^{-3}$ mg/ml (18), and a precursor, δ-aminolevulinic acid (ALA), was routinely administered to enhance the intracellular production of porphyrins when treating *E. coli* and other bacteria (19) by 400-420 nm blue light. In the absence of ALA, 407-420 nm blue light with a dose of 50 J/cm^2 did not exhibit significant bactericidal effects on *Staphylococcus aureus* (*S. aureus*), *A. baumannii* and *E. coli* (19). Also, it has been reported that the total amount of coproporphyrins was not a contributing factor of the antimicrobial efficacy of blue light treatment (20). Alternatively, pyocyanin, the prototypical green pigment produced by *P. aeruginosa* (21), has been suggested to serve as a photosensitizer upon blue light exposure (22, 23). Pyoverdine, a naturally occurring fluorescent pigment in *P. aeruginosa*, was also believed to undergo photodynamic reactions upon absorption of 415 nm light (24).

Very recently, our studies found that blue light at 460 nm is able to bleach staphyloxanthin (16), a ROS scavenger as well as an endogenous golden pigment residing in *S. aureus* functional membrane domains (25, 26), makes this pathogen vulnerable to low-concentration H_2O_2 (16). Follow-up studies using pulsed blue light have shown more effective capability of photobleaching of staphyloxanthin, which sensitizes *S. aureus* to a broad spectrum of antibiotics (17) and to silver nanoparticles (27). In an independent study, it was shown that photobleaching of another ROS scavenger and pigment, granadaene, by 430 nm light is able to reduce the virulence and increase the antimicrobial susceptibility of *Streptococcus agalactiae* (28). Collectively, these findings suggest an alternative working mechanism of antimicrobial blue light, which is based on photoinactivation of intrinsic ROS-scavenging molecules inside the pathogen.

It is well established that aerobic microorganisms produce ROS endogenously when flavin, quinol, or iron cofactors are autoxidized in the process of cellular metabolism and respiration (29). When bacteria are challenged with antibiotics or other stressors, a cascade of ROS could be generated (30, 31). Excess ROS damage DNA, certain metalloproteins, lipids, and other essential cellular components (32). To scavenge the excess ROS and maintain the intracellular homeostasis, bacteria have evolved to be armed with array of strategies. Of these, catalase, an enzyme with a turnover number of 2.8×10^6 molecules per second (33), very efficiently converts H_2O_2 into O_2 and water. For this reason, visualization of oxygen bubbles in the presence of H_2O_2 and Triton-X offered a simple method to quantify catalase activity (34). In the absence of catalase, Fenton reaction between H_2O_2 and iron would produce various radicals, such as $HO^{\cdot}$ and $HOO^{\cdot}$, and poses lethal threats to bacteria (35). Importantly, it was shown as early as 1965 that catalase could be inactivated by visible light (36), with the optical density at 405 nm (the primary absorption peak) diminishing as the irradiance continued. The underlying mechanism was presumed to be due to the dissociation of prosthetic heme groups from the tetramer protein (37). Nonetheless, whether photoinactivation of catalase could be harnessed to eliminate pathogenic bacteria is yet to be explored.

Here, we show that catalase expressed universally in common pathogens is a key target of antimicrobial blue light in the 400-420 nm optical window. Blue light illumination inactivates catalase by destroying the porphyrin rings. Using the same dose, nanosecond (ns) pulsed blue light at 410 nm induced more effective inactivation of catalase than the continuous-wave (CW) 410 nm irradiance. We further demonstrate that photoinactivation of catalase sensitized bacterial pathogens, both in planktonic form and biofilms, to exogenous non-bactericidal low-concentration H_2O_2. Moreover, photoinactivation of catalase sensitized pathogens to certain antibiotics that exert their lethal effects on bacteria partly through ROS-induced physiological alterations (38). Photoinactivation of catalase enhanced immune cell elimination of intracellular MRSA USA300 and *P. aeruginosa*. In a *P. aeruginosa*-induced mouse skin abrasion model, photoinactivation of catalase effectively reduced the pathogen burden. Taken together, our findings offer a new way to combat multi-drug resistant bacterial infections.

Results

Bacterial catalase can be inactivated by blue light irradiance

Catalase is a tetramer of 60,000-dalton subunits, containing four prosthetic heme rings per tetramer. As shown in **Figure 1A**, the porphyrin rings stay deep inside the hydrophobic pocket of catalase from *P. aeruginosa*. Since bovine liver catalase has been shown to be inactivated by visible light decades ago (36) but with unclear underlying mechanism, we asked whether and how catalase structure changes in the presence of light exposure near its absorption around 405 nm. For this purpose, Raman spectra of a dried bovine liver catalase film were obtained before and after 410 nm exposure. Catalase exhibits its prototypical peaks at 754 cm^{-1} and 1200 cm^{-1} to 1500 cm^{-1} because of porphyrin rings (**Figure 1B**) (39). Interestingly, the Raman intensity at those peaks drastically dropped after 410 nm exposure, indicating a possible dissociation of the heme ring from catalase.

To further understand the impact of 410 nm exposure on catalase, transient absorption microscopy was utilized to record the time-resolved photobleaching behavior of bovine liver catalase, and catalase inside MRSA USA300, *P. aeruginosa*, and *Salmonella enterica* (**supplementary Figure 1**). Samples were excited by a pump beam at wavelength of 410 nm and transient absorption signals were detected by a probe beam at wavelength of 520 nm. As shown in **supplementary Figure 1**, the transient absorption signal from bovine liver catalase decayed as the irradiance continued (**supplementary Figure 1**, **A**-**C**). Moreover, this decay (**supplementary Figure 1D)** follows a second-order photobleaching model (16), suggesting an interaction between heme rings within the tetramer. Consistently, photoinactivation of catalase from MRSA USA300 (**supplementary Figure 1E**), *P. aeruginosa* (**supplementary Figure 1F**), and *Salmonella enterica* (**supplementary Figure 1G**) followed the similar photobleaching trend as that of bovine liver catalase. Functionally, after 410 nm exposure, no apparent bubbles were observed when adding 0.3% H_2O_2 to the light-exposed catalase solution (**supplementary Video 1**). In summary, the enzyme-bound heme rings could be dissociated from the protein upon 410 nm irradiance, causing the protein to malfunction.

Next, we asked what is the optimal wavelength to inactivate catalase. To investigate this, we employed an OPO laser (Opolette 355, OPOTEK) and varied the laser wavelength under the same power density and dose. A catalase kit that quantifies the residual H_2O_2 was then used to indirectly measure the remaining catalase percent to evaluate the efficacy of light exposure. As shown in **Figure 1C**, 410-420 nm demonstrated the highest efficiency to inactivate bovine liver catalase (~50% inactivation at a dose of 15 J/cm^2). Catalase plays a dominant role in conversion of H_2O_2 into water and O_2 in bacteria (40). We adopted the same protocol to evaluate the remaining catalase percentage in stationary-phase MRSA USA300 (**Figure 1D**) and *P. aeruginosa* (**Figure 1E**). Consistently, 410-420 nm exposure most effectively attenuated the bacterial catalase activity. Therefore, 410 nm was utilized for catalase inactivation for the subsequent experiments.

Since photoinactivation of catalase is likely due to the dissociation of the heme rings from the protein following a second-order photobleaching model, we asked whether high-peak power pulsed (e.g., nanosecond) 410 nm (ns-410) blue light more effectively inactivates catalase

compared to the 410 nm continuous wave (CW-410). To answer this question, three experiments were conducted. First, we used the same catalase kit to quantify the H_2O_2 conversion efficacy of bovine liver catalase (**Figure 1F**), stationary-phase MRSA USA300 (**Figure 1G**), and stationary-phase *P. aeruginosa* (**Figure 1H**) after ns-410 and CW-410 blue light exposure, respectively. Our data repeatedly exhibited the pattern that ns-410 is significantly more effective for catalase inactivation compared to CW-410 (p<0.001). Second, Raman spectra of bovine liver catalase film dried on a glass substrate were obtained after ns-410 and CW-410 exposure. Noteworthy, under the same dose, ns-410 nm displayed a better capability to bleach catalase as Raman peaks at 754 cm^{-1} and 1200 to 1500 cm^{-1} drastically dropped (**Figure 1I**). Third, we compared the heights of oxygen bubble foams produced by catalase in the presence of H_2O_2 and Triton-X after ns-410 and CW-410 exposure at the same dose. As shown in **supplementary Figure 2**, ns-410 treated groups indeed showed much lower foam heights. Collectively, ns-410 exposure is more effective to inactivate catalase compared to CW-410. Notably, ns-410 exposure (10 Hz) also alleviates the heat accumulation issue which generally concomitants with long-time CW light exposure.

Photoinactivation of catalase sensitizes pathogenic bacteria to low H_2O_2 -concentrations

Since the primary role of catalase is to degrade H_2O_2 into water and oxygen, we then investigated whether photoinactivation of catalase renders bacteria vulnerable to H_2O_2. We tested the viability of MRSA USA300 and *P. aeruginosa* after different treatments (various light wavelength, light dose, and H_2O_2 concentration) by colony-forming units (CFU/ml) enumeration. H_2O_2 at 22 mM (or 0.075%) didn't show apparent bactericidal effect (**Figure 2, A-B**). Yet, 4-$\log_{10}$ reduction was achieved in the 410 nm plus H_2O_2 treated group, indicating a very strong synergy between 410 nm exposure and H_2O_2 for bacterial eradication.

It is noteworthy that the more recalcitrant stationary-phase *P. aeruginosa* PAO1 was completely eradicated by 410 nm plus H_2O_2 (**Figure 2B**). When tuning the irradiance wavelengths, the killing pattern is similar to that of catalase inactivation (**Figure 1, C-E**), suggesting catalase is a key target of blue light irradiance. In addition, ns-410 plus H_2O_2 treatment of MRSA USA300 outperformed CW-410 plus H_2O_2 treatment by approximately 3-$\log_{10}$ (**supplementary Figure 3A**). The combination treatment that made use of ns-410 achieved total eradication of *P. aeruginosa* PAO1, and outperformed the CW-410 plus H_2O_2 treatment (**supplementary Figure 3B**). These findings are in line with ns-410 being more efficient at inactivating catalase than CW-410 when using the same dose.

To further investigate whether it is catalase that primarily accounts for the synergy between 410 nm exposure and H_2O_2, we measured the viability of *E. coli* BW25113 along with its catalase-deficient mutants, *E. coli ΔkatG* (single mutant) and *E. coli ΔkatGE* (double mutant) under the same treatments. First, a time-killing CFU assay was conducted. Complete eradication of *E. coli* BW25113 was obtained in the ns-410 plus H_2O_2 treated group after two hours of incubation in PBS whereas 410 nm alone or H_2O_2 alone barely killed the bacteria (**Figure 2C**). The synergistic activity of a combination treatment is defined as a >2-$\log_{10}$ decrease in the CFU ml^{-1} compared to

that obtained with the most active agent alone (41). Therefore, there is an effective synergy between 410 nm blue light and H_2O_2.

Catalase-deficient *E. coli ΔkatG* and *E. coli ΔkatGE* have baseline susceptibility to H_2O_2 that are drastically higher compared to the isogenic wild type *E. coli* (**Figure 2**, **D-E**). The double mutant *E. coli ΔkatGE* exhibited no visible oxygen bubbles formation with the addition of H_2O_2 (**supplementary Figure 4**). Moreover, *E. coli ΔkatGE* exhibited similar susceptibility to H_2O_2 killing compared to wild type *E. coli* BW25113 exposed to ns-410 plus H_2O_2 in a time-kill assay, corroborating that catalase is the primary target of 410 nm light. More effective killing of the catalase-deficient mutants by 410 nm plus H_2O_2 was observed when compared to H_2O_2 treatment alone, suggesting the existence of additional molecular targets for 410 nm exposure.

To further confirm that catalase is the primary target of blue light and inactivation of its underlying function accounts for the synergy between 410 nm and H_2O_2, we further applied the treatments to *S. aureus Newman* along with its isogenic catalase-deficient mutant *S. aureus ΔkatA*. At a concentration of 22 mM, H_2O_2 eliminated less than 1-$\log_{10}$ of *S. aureus Newman* yet reduced around 4-$\log_{10}$ of *S. aureus ΔkatA* (**Figure 2F**). When combining 410 nm exposure and H_2O_2, total eradications were obtained for both *S. aureus Newman* (**Figure 2G**) and *S. aureus ΔkatA* (**Figure 2H**).

To consolidate the catalase inactivation hypothesis, we designed a rescue experiment in which catalase-deficient *E. coli ΔkatGE* was transformed with a pBad-HPII plasmid (Addgene 105839) to form into a rescue strain *E. coli ΔkatGE*::*pBad_katE*. Briefly, catalase expression of *E. coli ΔkatGE*::*pBad_katE* can be promoted in the presence of arabinose. After transformation, both wild type *E. coli* BW25113 and *E. coli ΔkatGE*::*pBad_katE* were cultured to log-phase. Then 30-J/cm^2 410 nm blue light was applied to treat *E. coli* BW25113 along with *E. coli ΔkatGE*::*pBad_katE*. Bacteria were then collected and incubated inside M9 media supplemented with 1% arabinose for 4 hours at 37°C. Subsequently, 2.2 mM H_2O_2 was added to the bacterial suspension, then followed by CFU assay to quantify residue viable bacterial cells.

As shown in **Figure 2, I-L**, the addition of arabinose has negligible effects on the CFU reduction of 410 nm plus H_2O_2-treated wild-type *E. coli* BW25113 under the applied treatment scenario (**Figure 2**, **I-J**). Interestingly, in the case of *E. coli ΔkatGE*::*pBad_katE*, with the presence of arabinose, there is only 1-$\log_{10}$ reduction of CFU/ml in the 410 nm plus H_2O_2-treated group (**Figure 2L**); whereas significantly more killing, 2-$\log_{10}$ reduction of CFU/ml, showed up in the 410 nm plus H_2O_2-treated group when promoter arabinose is absent (**Figure 2K**).

These data collectively demonstrate that catalase gene complementation can rescue catalase-deficient *E. coli ΔkatGE* in the presence of H_2O_2 stress, and further suggest that catalase is a major molecular target of 410-nm light exposure.

Catalase photoinactivation and H_2O_2 synergistically eradicate wide-ranging bacteria

Having established the synergy between 410 nm exposure and H_2O_2 in eradication of *E. coli*, MRSA USA300, and *P. aeruginosa*, we next asked whether this synergy works on other

pathogenic bacteria. In 2017, the world health organization published a list of twelve global priority pathogens, including *Acinetobacter baumannii* (*A. baumannii*), *P. aeruginosa*, *Salmonellae* etc. (42), most of which are catalase positive. It was reported that *A. baumannii* could induce severe mucous membrane infections or even bacteremia (43), *P. aeruginosa* has been the main culprit among patients with burn wounds, cystic fibrosis, acute leukemia, organ transplants (44). *Salmonellae*, the most commonly isolated foodborne pathogens, lead to approximately three million deaths worldwide due to *Salmonella* gastroenteritis (45). Therefore, we explored whether 410 nm exposure and H_2O_2 are effective against these life-threatening pathogens.

Consistently, we found that total eradications (around 8-$\log_{10}$ reduction) were achieved when the treatment was applied to stationary-phase *Salmonella enterica* ATCC 29630 (**Figure 3A**) and stationary-phase *E. coli* BW25113 (**Figure 3B**). 5-$\log_{10}$ reduction of stationary-phase *A. baumannii 1* (**Figure 3C**) was achieved in the 410 nm plus H_2O_2 treated group. Notably, this synergistic cocktail therapy achieved total eradication (around 8-$\log_{10}$ reduction) of multiple *P. aeruginosa strains* (**Figure 3, D-F**) and *Klebsiella pneumonia 1* strains (**Figure 3G**). We then asked if this synergy still holds for catalase-negative pathogens, e.g. *Enterococcus faecalis* (*E. faecalis 1*) (46). As shown in **Figure 3H**, H_2O_2 alone effectively killed *E. faecalis 1* by around 3-$\log_{10}$, but the enhanced bactericidal effect associated with 410 nm exposure was not as significant as that for catalase-positive pathogens. Taken together, 410 nm plus H_2O_2 can effectively eradicate wide-ranging life-threatening pathogens.

To query the translational potential of this synergistic therapy, we inquired whether short H_2O_2 (with higher concentration) incubation time remains effective to eliminate bacteria after 410 nm exposure. Prior to that, we evaluated the toxicity of 0.1% (w/v) H_2O_2 (30 mM, 2-min incubation), 410 nm exposure (75 J/cm^2), 410 nm exposure plus 0.1% H_2O_2 to a Chinese Hamster Ovary (CHO) cell line through MTT assay. A 0.1%~0.2% of H_2O_2 was chosen since it was reported that H_2O_2 in the commercially disinfectant formulations is in the range of 0.1% to 3% (47). As shown in **Figure 3I**, viability of CHO cells (around 80%) treated with 410 nm (75 J/cm^2) plus H_2O_2 (0.1%, 1-min incubation) was similar CHO cells treated with 410 nm or H_2O_2.

Hence, we moved next to interrogate the bactericidal effect of short treatment against log-phase MRSA USA30, *P. aeruginosa* PAO1 and *A. baumannii 1*. Enhanced killing of log-phase MRSA USA300 was observed with 410 nm plus H_2O_2 treatment compared to treatment with H_2O_2 or 410 nm alone (**Figure 3J**). Total eradication was achieved in the case of log-phase *P. aeruginosa* PAO1 (**Figure 3K**) and log-phase *A. baumannii 1* (**Figure 3L**) with 410 nm and 1-min 0.1%-0.2% H_2O_2. Log-phase MRSA USA300, *P. aeruginosa* PAO1 and *A. baumannii 1* were particularly sensitive to 410 nm exposure (**Figure 3L**) compared to the bacteria grown to stationary-phase, indicating possible variation in catalase expression with growth condition. Collectively, 410 nm plus short exposure to H_2O_2 are sufficient to achieve significant bacterial reduction with negligible toxicity.

Photoinactivation of catalase enhances microbicidal activity of H_2O_2-producing antibiotics

Significant intracellular H_2O_2 is produced upon treatment with ampicillin (β-lactam), gentamicin (aminoglycoside), and norfloxacin (fluoroquinolone) (38). Based on these prior studies, we reasoned that photoinactivation of catalase could enhance the efficacy of these antibiotics that induce ROS generation. To test our hypothesis, we firstly tested tobramycin, a representative of aminoglycoside that could indirectly enhance the intracellular production of H_2O_2 (48). Augmented killing effect was observed with 410 nm exposure plus tobramycin treatment of *E. coli* BW25113 compared with tobramycin treatment alone (**Figure 4A**). 410 nm exposure strengthened the bactericidal effect of tobramycin against *Salmonella enterica* by around 1-$\log_{10}$ (**Figure 4, B-C**), and did not enhance tobramycin killing of catalase-negative *Enterococcus faecalis* 1 (**Figure 4D**).

Per report, catalase-deficient *E. coli* mutants are more susceptible to fluoroquinolone ciprofloxacin when compared to their parent strain (49). We thus wondered whether photoinactivation of catalase could sensitize bacteria to ciprofloxacin. As shown in **Figure 4E**, photoinactivation of catalase indeed boosted the antimicrobial potency of ciprofloxacin to eliminate log-phase *P. aeruginosa* PAO1. Similar enhancement was observed for log-phase *A. baumannii* 2 (**Figure 4F**). Collectively, these findings suggest that photoinactivation of catalase augments the antimicrobial efficacy of at least some antibiotics that indirectly increase the intracellular H_2O_2 level.

Photoinactivation of catalase and H_2O_2 synergistically eliminate *P. aeruginosa* biofilms

Having shown effective synergy between photoinactivation of catalase and ROS-generating agents against both log- and stationary-phase planktonic bacteria, we next asked if the synergy can effectively eradicate biofilm-dwelling bacteria.

To address our query, we selected *P. aeruginosa* as a target since it is a notorious pathogen in burn wounds, chronic obstructive pulmonary disorder and cystic fibrosis (50). Extensive *P. aeruginosa* biofilm protect the bacterium from host defense, chemotherapy and conventional antimicrobial therapy, leading to undesirable disease burden on patients (51, 52).

To mimic clinical *P. aeruginosa* infections in which biofilm has a major presence, we adopted a CDC biofilm growth protocol which grows *P. aeruginosa* biofilms on a polypropylene coupon under continuous flow conditions (53). After forming robust biofilms, we applied treatments (untreated, H_2O_2 at a series of concentrations, 410 nm exposure (21 J/cm^2), 410 nm (21 J/cm^2) plus H_2O_2 (30-min incubation time)). Then we used a Live (SYTO 9)/Dead (Propidium iodide, PI) staining kit to image live/dead *P. aeruginosa* through a confocal microscope. As shown in **Figure 5A-D**, H_2O_2 treated groups barely have noticeable number of dead cells compared to the untreated group (**Figure 5I**). In comparison, drastic increase of dead bacteria number was observed in groups treated with 410 nm exposure plus H_2O_2 (**Figure 5, A-D, I**). 3D rendered images of *P. aeruginosa* biofilms (**supplementary Video 2**) further corroborated the synergistic effect between 410 nm exposure and H_2O_2 treatment to eliminate *P. aeruginosa* biofilms.

Of note, even after combining 410 nm and H_2O_2 at a concentration of 52.8 mM, full eradication still could not be achieved (around 70% elimination, **Figure 5E-H, J**), which may be attributed to the shielding conferred by the extracellular polymeric substances or quorum sensing inside the biofilms. Nonetheless, photoinactivation of catalase and H_2O_2 substantially eliminated *P. aeruginosa* in the biofilm setting, which suggests the potential for treating clinically relevant *P. aeruginosa* infections such as burn infections.

Photoinactivation of catalase assists macrophages to eliminate intracellular pathogens

Besides forming persistent biofilms, bacteria could also reside inside host immune or non-immune cells to evade antibiotic attack (54, 55). It has been reported that the minimal inhibitory concentrations (MICs) of intracellular MRSA is two orders of magnitude higher than those of free-living planktonic bacteria (55). Furthermore, *S. aureus* could proliferate within host phagocytic cells such as neutrophils and macrophages shortly after intravenous infection (56, 57). These viable intracellular *S. aureus* allow the infected cells to act as 'Trojan horses' for further dissemination to cause systematic infections (58). Therefore, more effective elimination of intracellular bacteria has the potential to improve current antibiotic therapeutics.

Staphylococcal catalase shields intracellular *S. aureus* by degrading H_2O_2 generated by murine peritoneal macrophages (59). Catalase has been reported to assist *Campylobacter jejuni* survive within macrophages as evidenced by extensive killing of catalase-deficient *Campylobacter jejuni* by macrophages (60). Neutrophils, as the first line of defense, can also harbor pathogens inside the phagocytic vacuoles (61), abetted by bacterial catalase that play a vital role in intracellular survival (62). Therefore, we wondered whether photoinactivation of catalase could boost immune mechanisms of eliminating intracellular pathogens.

Thus, we infected the mice macrophage cell line RAW 264.7 with log-phased MRSA USA300 and 410 nm pre-treated log-phase MRSA USA300 at a multiplicity of infection (MOI) of 100 for one hour. After eliminating MRSA USA300 outside the macrophages by incubating with gentamicin for one hour, we adopted a protocol to label the live (SYTO 9)/dead (PI) MRSA USA300 inside the macrophages (63). As shown in **Figure 6A-C**, there was a large number of live MRSA USA300 in the cytoplasm of macrophages after phagocytosis of untreated MRSA USA300. In comparison, the number of dead 410 nm pre-exposed MRSA USA300 is significantly increased inside macrophages (**Figure 6D-F**). We performed quantitative analysis of live/dead MRSA USA300 inside single macrophage from fifty macrophages (**Figure 6G-H**). There was a clear difference in the number of dead bacteria between the two groups.

To further confirm that photoinactivation of catalase enhances macrophage elimination of intracellular pathogens, we enumerated intracellular bacteria by lysing macrophages with 0.1% Triton-X for 3 min after 4-h infection. As shown in **Figure 6I**, there was an approximate 2-$\log_{10}$ reduction of intracellular MRSA USA300 burden in the 410 nm exposure (15 J/cm^2) group. Consistently, a 1.5-$\log_{10}$ reduction of intracellular *P. aeruginosa* was obtained in macrophages infected with 410 nm (15 J/cm^2)-exposed *P. aeruginosa* (**Figure 6J**). In addition, we also tried to treat macrophages with blue light after internalization of *P. aeruginosa*, 410 nm-treated group

consistently demonstrated lower intracellular bacterial burden (**supplementary Figure 5A**). Also, we found that utilization of a NOX2 inhibitor diminished this difference (**supplementary Figure 5B**), which suggests that ROS burst inside macrophages is crucial for efficient elimination of intracellular bacteria. We showed that 410 nm exposure didn't cause significant toxicity to non-infected RAW 264.7 cells (**Figure 6K**). Collectively, the results of the confocal live/dead imaging along with the CFU assay suggest that 410 nm exposure can facilitate host immune killing of intracellular pathogens.

Photoinactivation of catalase reduces *P. aeruginosa* burden in a mouse skin abrasion model

Towards clinical translation, we further evaluated the synergy between photoinactivation of catalase and H_2O_2 using a bacterial infection murine model. Specifically, we adopted a *P. aeruginosa*-infected mouse skin abrasion model (64) to mimic clinical *P. aeruginosa*-mediated skin infection. Briefly, we applied 10^8 CFU of *P. aeruginosa* to abrazed mouse skin for three hours. After the wound was established, 410 nm blue light (120 J/cm^2), 0.5% H_2O_2, 0.5% H_2O_2 plus 410 nm (120 J/cm^2) were independently applied to the infected area for two times before euthanasia (**Figure 7A**). Wound tissues from the euthanized mice were then subjected to homogenization in order to enumerate CFU. As shown in **Figure 7B**, the untreated mice wound has around 10^6 CFU/ml of *P. aeruginosa*, and 410 nm light alone significantly (p=0.02) reduced bacterial burden by around 60%. Noticeably, 410 nm light exposure significantly enhanced (p=0.0002) the bactericidal effect of 0.5% H_2O_2 against *P. aeruginosa* by one order of magnitude.

To evaluate whether our combinational treatment causes skin damage, we collected the mouse skin after applying 410 nm at the same dose plus 0.5% H_2O_2. We then performed the hematoxylin and eosin staining and histology analysis. As shown in **Figure 7C-D**, epidermis, dermis and subcutaneous tissues were not different from the untreated control.

To evaluate whether longitudinal blue light treatment could generate any effect on mouse physiology, we applied three-consecutive-day blue light treatment after *P. aeruginosa* infection (once a day). Meanwhile, wound size, body temperature and weight were monitored and recorded each day after treatment. As shown in **supplementary Figure 6**, we didn't observe significant changes in the mice temperature and body weight among different treatment groups over time. Interestingly, there was a significant difference regarding the wound size **(supplementary Figure 6C**) between the untreated group and combination (410 nm plus H_2O_2) treated group. The combination treated group showed smaller wound size and better wound healing outcome. Our data further indicated that mice didn't develop bacteremia three days after the infection, even in the untreated group, as their activity and mobility behaved normally.

Collectively, these *in vivo* data provide the foundation for exploring the clinical utility of our catalase-targeted therapy against multidrug-resistant bacterial infections.

Discussion

Since the discovery of penicillin in 1928 by Alexander Fleming (65), there was a golden age (from 1940s to 1960s) for the discovery of antibiotics, most of which remain in clinical use today (66). Yet, imprudent usage of antibiotics speeded up the natural selection of drug-resistant bacteria (67). In the past decades, the ever-rising emergence of multidrug-resistant bacteria has been an alarming threat worldwide. Moreover, the pace of antibiotic development hasn't kept up with antibiotic resistance development. Therefore, novel alternative approaches are highly desired to combat the new waves of multidrug-resistant bacterial infections.

It has been reported that catalase serves an important virulence function for intracellular bacteria evasion of neutrophil phagocytosis (68). *E. coli* pretreated with phenazine methosulfate showed a nine-fold increase of catalase synthesis, and demonstrated resistance against neutrophil killing (69). With catalase expression, *S. aureus* has significantly higher viability in the presence of human neutrophils (70). Besides neutrophils, staphylococcal catalase protects intracellular bacteria by neutralizing H_2O_2 produced by macrophages (59). Not only does catalase plays an important role in host-microbe interaction, it has been shown that catalase expression contributes significantly to the survival of catalase-positive *S. aureus* against catalase-negative *Streptococcus pneumoniae* in a murine model of nasal colonization (71). Therefore, catalase inactivation could deprive pathogenic bacteria of an essential armament.

In this paper, we identified catalase as a key molecular target of blue light for a wide range of pathogens. Through spectroscopic study, we found that catalase can be functionally inactivated by blue light, especially at 410 nm. We further demonstrated that photoinactivation of catalase renders wide-ranging pathogenic bacteria and *P. aeruginosa* biofilms highly susceptible to subsequent H_2O_2 or H_2O_2-producing agents. The close correlation between catalase inactivation and its bacterial killing efficiency, the catalase gene complementation study, further validate that catalase is a major molecular target of blue light. In addition, photoinactivation of catalase significantly enhances macrophage killing of intracellular pathogens, and further reduces bacterial burden in a *P. aeruginosa*-infected mouse abrasion model without causing significant skin damage. Towards clinical translation, the synergy between photoinactivation of catalase and H_2O_2/antibiotics is most suitable for superficial bacterial infections due to limited penetration depth of 410 nm light. To improve the treatment depth, tissue-clearing agent can be applied to enhance the light penetration through the skin. Alternatively, up-conversion nanoparticles can be employed by tuning the excitation wavelength from blue light to near infrared light (72). For intra-body infections such as urinary tract infections, light-emitting catheters can be designed to deliver the blue light to the infection site.

We found that ns-410 nm blue light is significantly more effective at inactivating catalase than CW-410 nm using the same dose. Moreover, ns-410 nm plus H_2O_2 kills more bacteria compared to CW-410 nm plus H_2O_2. Enhanced bacterial killing probably comes from the second-order photobleaching behavior of catalase under 410 nm irradiance, where prosthetic heme rings inside the tetramer might react with each other to detach from protein matrix. Raman spectra of catalase before and after 410 nm treatment hinted the porphyrin changes or dissociation. As an additional benefit, ns-410 nm exposure could also eliminate the heating issue which is always accompanied

by CW-410 nm irradiance. It has been reported that heat dissipation is in the range of microsecond (73), and ns-410 nm here was modulated at a frequency of 10 Hz, which could efficiently address the heat accumulation issue. In short, ns-410 nm might have better potential for clinical translation to treat multi-drug resistant bacterial infections compared to CW-410 nm.

We also found that stationary-phase pathogens such MRSA USA300 or *P. aeruginosa* are significantly more susceptible to subsequent H_2O_2 attack after photoinactivation of catalase. Stationary-phase and non-dividing pathogens (e.g., persisters) are known to cause persistent infections such as endocarditis or osteomyelitis or biofilm-associated infections (74). The persisting pathogens appear to be metabolically dormant and thrive under nutrition depleted environment (75). The dormant bacteria demonstrate higher levels of tolerance and persistence to antimicrobial agents when compared to metabolically active planktonic bacteria (76). Therefore, alternative approaches to combat stationary-phase pathogens and persisters are important. Catalase activity has been reported to be increased in some stationary-phase bacteria (77). Our novel approach demonstrated bactericidal efficacy against a broad range of stationary-phase pathogens. Thus, we believe this synergistic treatment will presumably work on the persisters as well.

We showed that photoinactivation of catalase also enhances immune cell elimination of intracellular pathogens. Bacterial catalase promotes intracellular pathogens survival inside immune cells (78). As shown in **Figure 6A**, as significant portion of MRSA USA300 remained alive after internalization by macrophages. After photoinactivation of catalase, both intracellular MRSA USA300 and *P. aeruginosa* burden significantly reduced. Photoinactivation of catalase also significantly reduced bacterial load in the mouse skin abrasion model (**Figure 7B**) without causing skin damage. Although catalase is a major molecular target of blue light, it is not the only target of 410 nm irradiance since some H_2O_2 killing of catalase-deficient *E. coli* mutants and *S. aureus* mutants was still observed after 410 nm blue light treatment (**Figure 2**). This finding indicates that molecular targets of the 410 nm light other than catalase likely exist. Noteworthy, there are other endogenous molecules which are intrinsic to specific bacteria already revealed as molecular targets of blue light. For example, researchers have demonstrated endogenous pigments are essential virulence factors for microbes (79). Moreover, many of them can be inactivated by photons, thus rendering microbes highly susceptible to exogenous reactive oxygen species (16, 17). Therefore, intrinsic pigments can be explored to find out other molecular targets. Another intriguing direction is to interrogate the possible correlation between catalase level and drug resistance. If drug-resistant bacteria show the propensity to express higher level of catalase compared to susceptible one, photoinactivation of catalase might provide a universal approach to disarm drug-resistant pathogens. Collectively, our findings reveal a significant mechanism of antimicrobial blue light and fueled a novel catalase-targeted strategy to combat clinical multidrug-resistant bacterial infections.

Methods

Blue light source: Pulsed blue light was administered using a Opolette HE 355 LD laser (OPOTEK). The nanosecond pulsed laser is tunable from 410 nm to 2200 nm, has a repetition rate of 10-20 Hz, and a pulse width of ~5-10 ns. Using a collimator attached to an optical fiber, the diameter of the laser beam was expanded to 10 mm. With these set parameters, the pulsed laser provides a power output ranging from 25 to 100 mW/cm^2, depending on the laser wavelength used. Continuous wave blue light was delivered through a mounted 405 nm blue light LED (M405L4, Thorlabs) with an adjustable collimation adapter (SM2F32-A, Thorlabs) focusing the illumination region to a ~1 cm^2 region. A T-Cube LED driver (LEDD1B, Thorlabs) allowed for adjustable light fluencies up to 400 mW/cm^2.

Bacterial strains and cell lines: Bacterial strains MRSA (USA300), *P. aeruginosa* PAO1 (ATCC 47085), *P. aeruginosa* 2 (ATCC 1133), *P. aeruginosa* 3 (ATCC 15442), *P. aeruginosa* 4 (ATCC 9027), *S. enterica* 2 (ATCC 700720), *S. enterica* 3 (ATCC 13076), *E. coli* 1 (BW25113), *K. pneumoniae* 1 (ATCC BAA 1706), *A. baumannii* 1 (ATCC BAA 1605), *A. baumannii* 2 (ATCC BAA-747), *E. faecalis* 1 (NR-31970), and *E. faecalis* 2 (HM-335) were provided by the Dr. Mohamed N. Seleem at Virginia Tech. *E. coli* mutants (*ΔahpC*, *ΔkatG*, *ΔkatE*, *ΔkatGE*) were provided by the Dr. Xilin Zhao Group at Rutgers University. All cell lines used in this study, including the RAW 264.7 murine macrophages, chinese hamster ovary (CHO) cells were purchased directly from the American Type Culture Collection (ATCC).

Transient absorption imaging of real-time photobleaching of catalase: As described previously(80), an optical parametric oscillator synchronously pumped by a femtosecond pulsed laser generated the pump (820 nm) and probe (1040 nm) pulse trains. The pump and probe beams were then frequency-doubled via the second–harmonic generation process to 410 nm and 520 nm through barium borate crystals, respectively. Temporal delay between the pump and probe pulses was controlled through a motorized delay stage. The pump beam intensity was modulated with an acousto-optic modulator. The intensity of each beam was adjustable through the combination of a half-wave plate and a polarization beam splitter. Thereafter, pump and probe beams were collinearly combined and directed into a laboratory-built laser scanning microscope. Through the nonlinear process in the sample, the modulation of pump beam was transferred to the unmodulated probe beam. Computer-controlled scanning galvo mirrors were used to scan the combined laser beams in a raster scanning approach to create microscopic images. The transmitted light was collected by an oil condenser. Subsequently, the pump beam was spectrally filtered by an optical filter, and the transmitted probe intensity was detected by a photodiode. A phase-sensitive lock-in amplifier (Zurich Instruments) then demodulated the detected signal. Therefore, pump-induced transmission changes in the probe beam versus the temporal delay can be measured. This change over time delay shows different time-domain signatures of a chromophore, thus offering the origin of the chemical contrast.

Raman spectra of catalase before and after 410 nm irradiance: Raman spectra of catalase before and after 410 nm exposure were acquired under a Horiba Raman system (1221, LABRAM

HR EVO, Horiba) with a 40× objective under the excitation of 532 nm. Raman spectra were obtained under a 20-s acquisition time with a 10% laser ND filter. Bovine liver catalase (C9322, Sigma Aldrich) was dissolved in sterile distilled H_2O (4 U/mL) and then air-dried onto a clean cover slide. Changes in catalase structure were evaluated by examining decreases in specific Raman peaks following light treatment.

Quantitation of remaining active catalase: Measurement of active catalase was primarily quantified through the use of an Amplex Red Catalase Assay (A22180, Thermo Fisher Scientific). Briefly, solutions containing catalase (either bovine liver catalase or catalase-positive bacteria inoculum) were treated with blue light, after which 25 µL of the light treated solution was incubated with 40 µM of H_2O_2 for 30 minutes at room temperature within a 96-well plate. Following H_2O_2 treatment, 50 µL of a reaction stock containing 100 µM of Amplex Red and 0.4 U/mL of horseradish peroxidase were added to each well and the combination was incubated for 30 minutes at 37°C. Following incubation, the fluorescence of each well was measured using an excitation wavelength of 543 nm and an emission wavelength of 585 nm. In addition to the light treated samples, a phosphate buffered saline (PBS) negative control and an untreated positive control also treated with the assay to determine the remaining catalase percentage. Active catalase percent was calculated through the following equation:

$$Remaining\ catalase\ \% = \frac{I_{PBS} - I_{treated}}{I_{PBS} - I_{untreated}} \times 100\ \%$$

CFU enumeration assay to evaluate the synergy between photoinactivation of catalase and ROS-generating agents: *P. aeruginosa* and MRSA were cultured overnight in TSB at 37°C within a shaking incubator (250rpm). The next day, the bacteria were suspended in 1×PBS (OD_{600} = 1.0), after which a 10 µL of aliquot was placed on a glass cover slide and then treated with ns-410 nm or CW-410 nm. Following light treatment, the droplet was transferred to a tube containing either PBS or 22 mM of H_2O_2 diluted in PBS. Samples were incubated for 30 minutes under 37°C, after which the bacteria samples were 10-fold serially diluted within a 96-well plate, plated on tryptic soy agar plates overnight, and then CFU enumerated the next day. Subsequent experiments testing the synergy between ns-410 or CW-410 blue light and different concentrations of H_2O_2 were also performed on other stationary phase bacteria including *E. coli*, *P. aeruginosa*, MRSA, *A. baumannii*, *S. enterica*, *K. pneumoniae*, and *E. Faecalis*. Similar to previous CFU synergy experiments, wild type *E. coli* (BW25113), an alkyl hydroperoxide reductase negative mutant strain (*ΔahpC*), and three catalase negative mutants (*ΔkatG*, *ΔkatE*, *ΔkatGE*) were all cultured overnight in TSB at 37°C within a shaking incubator (250rpm). Following incubation, bacteria strains were suspended in 1×PBS (OD_{600} = 1.0). A 20 µL aliquot of bacteria was placed on a glass coverslip and exposed to ns-410 light (32 mW/cm^2, 14 J/cm^2). The droplet was then removed and diluted with 780 µL of PBS. This light treated sample, alongside a non-light exposed sample, was treated with 2.2 mM of H_2O_2. Samples were shaken and incubated at 37°C for up to 2 hours. During the incubation, 60 µL aliquots would be removed from each sample tube for serial dilatation and CFU plating at the 20 minute, 40 minute, 1 hour, 1.5 hour, and 2-hour time points.

Mammalian cell toxicity assay: To evaluate the potential toxicity of 410 nm exposure and short term, high concentration H_2O_2 exposure against mammalian cells, a MTT assay was performed using Chinese Hamster Ovary (CHO) cell line (ATCC) and noninfected RAW 264.7 cells. RAW 264.7/CHO cells were cultured in Dulbecco's Modified Eagle Medium (DMEM, Gibco) alongside 10% fetal bovine serum (FBS) until 90% confluence was achieved. Once high confluence was established, cells were removed through trypsin treatment, quantified with a cell counter, and diluted in DMEM media to a final cell concentration of 1×10^6 cells/mL. 100 µL of cell media were added to each well of a 96-well plate, providing each well with 1×10^5 cells per well. Each well was supplemented with an additional 100 µL of DMEM media to bring the final volume of each well to 200 µL. HEK/CHO cells were then incubated overnight at 37°C with 5% CO_2 in order to allow the cells to adhere to the wells. Following the replacement of DMEM with PBS, light treated wells were exposed to 75 J/cm^2 of 410 nm LED light (250 mW/cm^2). After light exposure, PBS was removed and replaced with DMEM. For the H_2O_2 treatment groups, 0.1% H_2O_2 suspended in DMEM was added to the H_2O_2 treatment groups for 1 minute, after which the H_2O_2 containing media was removed and the wells were washed twice with PBS. Identical two-fold PBS washing was also applied to the other treatment groups to maintain experimental consistency. After that, the PBS was replaced with fresh DMEM and incubated overnight at 37 C with 5% CO_2 to allow for the surviving cells to recover from the stress exerted by the treatment. The next day, an MTT viability assay was performed based on previously established protocols. MTT absorbance measurements were quantified via plate reader at 590 nm. The assay was performed in replicates of N=4.

Preparation of catalase rescue strain *E. coli ΔkatGE*::*pBad_katE*: An *E. Coli* DH5α strain expressing an arabinose regulated pBAD-HPII (katE catalase) plasmid (AddGene, 105839) was cultured and a GeneJET Plasmid Miniprep Kit (ThermoFisher Scientific, K0503) was used to isolate the pBAD-HPII plasmid. A TransformAid Bacterial Transformation Kit (ThermoFisher Scientific, K2711) was then used to transform the double catalase knockout of *E. Coli ΔkatGE* and insert the arabinose regulated catalase plasmid to form a catalase rescue strain *E. coli ΔkatGE*::*pBad_katE*. Then both wild type *E. coli* BW25113 and *E. coli ΔkatGE*::*pBad_katE* were cultured at 37°C to log phase and then resuspended to PBS. A 10 µL aliquot was treated to CW-410 (30 J/cm^2) and then incubated in a M9 minimal media containing 1% arabinose for 4 hours at 37°C. Following the incubation, the bacterial suspension was treated with 2.2 mM of H_2O_2 for 30 minutes and then plated on agar plates. CFU enumeration was recorded for phenotypic response comparisons.

CFU assay between photoinactivation of catalase and certain antibiotics: For each antibiotic tested, bacterial strains were usually pre-cultured in antibiotics prior to light exposure of subsequent incubation. To summarize, 1 mL of overnight cultured bacteria was centrifuged and suspended in 1 mL of fresh TSB media supplemented with either 10 µg/mL of tobramycin (Sigma Aldrich, T4014) or 0.1 µg/mL of ciprofloxacin (Sigma Aldrich, 17850). Following pre-culture treatment, the bacterial solution was spun down and resuspended in 1×PBS. A 10 µL aliquot of the bacterial preculture stock was then placed on a coverslip and exposed to ns-410 with a dose of 18 J/cm^2, after which the aliquot was transferred to 990 µL of fresh TSB supplemented with either

2 μg/mL of tobramycin or 0.1 μg/mL of ciprofloxacin and incubated at 37°C for up to 6 hours. CFU dilution and enumeration was taken at various time points during the incubation period.

Intracellular bacteria assay: In all experiments, bacteria were cultured in TSB. To assess intracellular killing with macrophage RAW 264.7 cell line (ATCC), MRSA USA300 or *P. aeruginosa* was taken from an exponentially growing culture and washed in PBS. Macrophages were pre-washed with serum-free DMEM media immediately before infection and infected by MRSA USA300/P. *aeruginosa* with and without 410 nm treatment. Then co-culture was incubated at 37 °C in a humidified tissue culture incubator with 5% CO_2 to permit phagocytosis of the bacteria. After 2-4 h, the infection mix was removed and replaced with normal growth media (DMEM supplemented with 10% FBS, 10 mM HEPES) and gentamycin was added at 50 μg/ml to prevent growth of extracellular bacteria for 1 hour. Two approaches were utilized to evaluate the difference. The first one was to utilize a Live/Dead confocal staining assay to visualize the live and dead bacteria inside macrophages, respectively. Briefly, after fixation with 10% formalin following gentamicin treatment, samples were permeabilized with 0.1% Triton-X for 3 min at r.t. After that, a Live/Dead fluorescence kit (Thermo Fisher Scientific, L7007) was utilized to stain the intracellular bacteria. Confocal laser scanning microscope (FV3000, Olympus) was employed to visualize stained samples. The second one was to enumerate the intracellular CFU. In brief, co-cultures were permeabilized with 0.1% Triton-X for 3-5 min, vigorous pipetting was conducted to release intracellular bacteria. 10-fold serial dilution was immediately applied to count the viable intracellular bacteria.

To quantify the impact of NOX inhibitor on elimination of intracellular bacteria by macrophages, macrophages were firstly exposed to diphenyleneiodonium chloride (DPI, Sigma Aldrich, D2926) for one hour. DPI is a known inhibitor of the NOX enzymes responsible for the ROS burst in macrophages. After that, *P. aeruginosa* with/without 410 nm exposure infected macrophages at a MOI of 20. Two hours after infection, gentamicin was added to the co-culture to remove extracellular bacteria for one hour. Then intracellular bacteria were quantified after permeabilization with 0.1% Triton-X for 3 min and serial dilution.

***P. aeruginosa* biofilm assay:** As reported previously(10), *P. aeruginosa* biofilms were formed onto a coupon through a CDC biofilm reactor for two days. After the biofilm formation, different treatment schemes were then applied. Live/dead fluorescence staining was utilized to evaluate the treatment efficacy. Confocal laser scanning microscope was then employed to capture the counterstained images.

***In vivo* murine infection model and histology:** Twenty BALB/c mice (Jackson Laboratories, 000651) were placed under anesthesia and a #15 sterile scalpel was used to generate a 1 cm^2 abrasion wound by carefully scraping the epidermis of the skin without drawing blood. Once the wound had been generated, a 10 μL aliquot containing 10^8 CFU of log-phase PAO1 in PBS was placed onto the abrasion wound and spread evenly across the wound with a pipette tip. Once the droplet had dried, the mice were returned to their cage to allow the mice to recover from their abrasion wound and to provide time for the bacteria to infect the wound. The 20 mice were then divided into four treatment groups, each consisting of 5 mice (N = 5): Untreated, 410 nm treated,

H_2O_2 treated, and 410 nm plus H_2O_2 treated. Light treatment was applied by positioning mice under 200 mW/cm^2 (ANSI standard) 410 nm LEDs and exposing their bacteria infected wounds to 120 J/cm^2 of blue light. For H_2O_2 treatment, 10 µl of 0.5% H_2O_2 was evenly distributed on the infected wounds and allowed to naturally dry. Combination treatment consisted of the application of previously described light treatment followed by H_2O_2 treatment. Treatments were applied to mice twice over the course of 15 hours, with the first treatment being applied 3 hours following infection and the second treatment being applied 12 hours after the first treatment. 3 hours after the second treatment, mice were euthanized and wound tissue was harvested, homogenized, and serially diluted. CFU enumeration was performed on *P. aeruginosa*-specific cetrimide agar plates (Sigma Aldrich, 22470).

The potential phototoxicity of the treatment on the skin was evaluated by applying the combination treatment on healthy, non-wounded skin regions present on the combination treated mice. This healthy region of the skin would receive the same two treatments as the wound site, and during tissue harvesting, this region was excised and preserved in 10% buffered formalin alongside a collection of unwounded skin samples from the untreated mice. Formalin fixed samples were submitted to the Boston University Experimental Pathology Laboratory Service Core for histology processing and hematoxylin and eosin (H&E) staining. Histology slides were then visualized under an inverted microscope through a 60× objective.

Author contributions:

P.-T.D. and J.-X.C. conceived the synergistic therapeutic treatment between photoinactivation of catalase and H_2O_2 or certain antibiotics. P.-T.D., Y.F.Z., J.H. discovered that catalase from catalase-positive bacteria could be ubiquitously inactivated by 410 nm. P.-T.D. characterized catalase photoinactivation and intracellular bacteria assay. P.-T.D., S.J. and J.H. conducted the *in vitro* CFU assay. J.H. conducted the biofilms experiment. P.-T.D., S.J. and Y.W.Z. conducted the *in vivo* mice abrasion experiments and histology assay. P.-T.D. and J.-X.C. co-wrote the manuscript. G.L. provided constructive suggestions over the project and manuscript. All authors read and commented on the manuscript.

Acknowledgments:

This work was partly supported by R01AI141439 to J.-X.C. We kindly acknowledge Dr. Xilin Zhao from Rutgers University (New Brunswick, New Jersey) for providing the catalase-deficient *E. coli* strains. Research reported in this publication was also supported by the Boston University Micro and Nano Imaging Facility and the office of the director, National Institute of Health, National Institute of Health under Award Number S10OD024993.

Statistics:

Statistical analysis was conducted through student's unpaired *t*-test (two groups) and One-way ANOVA (three or more groups). *** means significantly different with a p-value < 0.001. ** means significantly different with a p-value < 0.01. * means significantly different with a p-value < 0.05. ns means no significance.

Study approval:

Mice abrasion model experiment was approved by the Boston University Animal Care and Use Committee and were in accordance with National Institutes of Health Guidelines.

Competing interests:

The authors have declared that no conflict of interest exists.

References

1. Prestinaci F, Pezzotti P, and Pantosti A. Antimicrobial resistance: a global multifaceted phenomenon. *Pathog Glob Health.* 2015;109(7):309-18.
2. Ventola CL. The antibiotic resistance crisis: part 1: causes and threats. *P T.* 2015;40(4):277-83.
3. Willyard C. The drug-resistant bacteria that pose the greatest health threats. *Nature.* 2017;543(7643):15.
4. Fair RJ, and Tor Y. Antibiotics and bacterial resistance in the 21st century. *Perspect Medicin Chem.* 2014;6:25-64.
5. Leanse LG, Dong P-T, Goh XS, Lu M, Cheng J-X, Hooper DC, et al. Quinine enhances photo-inactivation of Gram-negative bacteria. *J Infect Dis.* 2020;221(4):618-26.
6. Wang Y, Wang Y, Wang Y, Murray CK, Hamblin MR, Hooper DC, et al. Antimicrobial blue light inactivation of pathogenic microbes: State of the art. *Drug Resist Updat.* 2017;33-35:1-22.
7. Ashkenazi H, Malik Z, Harth Y, and Nitzan Y. Eradication of *Propionibacterium acnes* by its endogenic porphyrins after illumination with high intensity blue light. *FEMS Immunol Med Microbiol.* 2003;35(1):17-24.
8. Hamblin MR, Viveiros J, Yang C, Ahmadi A, Ganz RA, and Tolkoff MJ. *Helicobacter pylori* accumulates photoactive porphyrins and is killed by visible light. *Antimicrob Agents Chemother.* 2005;49(7):2822-7.
9. Morici P, Battisti A, Tortora G, Menciassi A, Checcucci G, Ghetti F, et al. The *in vitro* photoinactivation of *Helicobacter pylori* by a novel LED-based device. *Front Microbiol.* 2020;11(283).
10. Ferrer-Espada R, Liu X, Goh XS, and Dai T. Antimicrobial blue light inactivation of polymicrobial biofilms. *Front Microbiol.* 2019;10(721).
11. Amin RM, Bhayana B, Hamblin MR, and Dai T. Antimicrobial blue light inactivation of *Pseudomonas aeruginosa* by photo-excitation of endogenous porphyrins: *In vitro* and *in vivo* studies. *Lasers Surg Med.* 2016;48(5):562-8.
12. Leanse LG, Harrington OD, Fang Y, Ahmed I, Goh XS, and Dai T. Evaluating the potential for resistance development to antimicrobial blue light (at 405 nm) in Gram-negative bacteria: *In vitro* and *in vivo* studies. *Front Microbiol.* 2018;9(2403).
13. Tomb RM, Maclean M, Coia JE, MacGregor SJ, and Anderson JG. Assessment of the potential for resistance to antimicrobial violet-blue light in *Staphylococcus aureus*. *Antimicrob Resist Infect Control.* 2017;6(1):100.
14. Leanse LG, Goh XS, and Dai T. Quinine improves the fungicidal effects of antimicrobial blue light: Implications for the treatment of cutaneous *Candidiasis*. *Lasers Surg Med.* 2020;52(6):569-75.
15. Moorhead S, Maclean M, Coia JE, MacGregor SJ, and Anderson JG. Synergistic efficacy of 405 nm light and chlorinated disinfectants for the enhanced decontamination of *Clostridium difficile* spores. *Anaerobe.* 2016;37:72-7.
16. Dong P-T, Mohammad H, Hui J, Leanse LG, Li J, Liang L, et al. Photolysis of staphyloxanthin in methicillin-resistant *Staphylococcus aureus* potentiates killing by reactive oxygen species. *Adv Sci (Weinh).* 2019;6(11):1900030.
17. Hui J, Dong P-T, Liang L, Mandal T, Li J, Ulloa ER, et al. Photo-Disassembly of Membrane Microdomains Revives Conventional Antibiotics against MRSA. *Adv Sci (Weinh).* 2020;7(6):1903117.
18. Keshishyan ES, Zaporozhtseva ZV, Zenina OM, and Zrodnikov VS. Photodynamic inactivation of bacteria in vitro under the effect of blue light. *Bull Exp Biol Med.* 2015;158(4):475-7.
19. Nitzan Y, Salmon-Divon M, Shporen E, and Malik Z. ALA induced photodynamic effects on Gram positive and negative bacteria. *Photochem Photobiol Sci.* 2004;3(5):430-5.
20. Kim M-J, and Yuk H-G. Antibacterial mechanism of 405-nanometer light-emitting diode against *Salmonella* at refrigeration temperature. *Appl Environ Microbiol.* 2017;83(5):e02582-16.

21. Lau GW, Hassett DJ, Ran H, and Kong F. The role of pyocyanin in *Pseudomonas aeruginosa* infection. *Trends Mol Med.* 2004;10(12):599-606.
22. Orlandi VT, Bolognese F, Chiodaroli L, Tolker-Nielsen T, and Barbieri P. Pigments influence the tolerance of *Pseudomonas aeruginosa* PAO1 to photodynamically induced oxidative stress. *Microbiology.* 2015;161(12):2298-309.
23. Lipovsky A, Nitzan Y, and Lubart R. A possible mechanism for visible light-induced wound healing. *Lasers Surg Med.* 2008;40(7):509-14.
24. Sabino CP, Wainwright M, dos Anjos C, Sellera FP, Baptista MS, Lincopan N, et al. Inactivation kinetics and lethal dose analysis of antimicrobial blue light and photodynamic therapy. *Photodiagnosis Photodyn Ther.* 2019;28:186-91.
25. García-Fernández E, Koch G, Wagner RM, Fekete A, Stengel ST, Schneider J, et al. Membrane microdomain disassembly inhibits MRSA antibiotic resistance. *Cell.* 2017;171(6):1354-67.e20.
26. Liu C-I, Liu GY, Song Y, Yin F, Hensler ME, Jeng W-Y, et al. A cholesterol biosynthesis inhibitor blocks *Staphylococcus aureus* virulence. *Science.* 2008;319(5868):1391-4.
27. Jusuf S, Hui J, Dong P-T, and Cheng J-X. Staphyloxanthin photolysis potentiates low concentration silver nanoparticles in eradication of methicillin-resistant *Staphylococcus aureus*. *J Phys Chem C.* 2020;124(9):5321-30.
28. Jusuf S, Dong P-T, Hui J, Ulloa ER, Liu GY, and Cheng J-X. Granadaene photobleaching reduces the virulence and increases antimicrobial susceptibility of *Streptococcus agalactiae*. *Photochem Photobiol.* 2021;97(4):816-25.
29. Yang L, Mih N, Anand A, Park JH, Tan J, Yurkovich JT, et al. Cellular responses to reactive oxygen species are predicted from molecular mechanisms. *Proc Natl Acad Sci U S A.* 2019;116(28):14368-73.
30. Zhao X, and Drlica K. Reactive oxygen species and the bacterial response to lethal stress. *Curr Opin Microbiol.* 2014;21:1-6.
31. Dwyer DJ, Kohanski MA, and Collins JJ. Role of reactive oxygen species in antibiotic action and resistance. *Curr Opin Microbiol.* 2009;12(5):482-9.
32. Ezraty B, Gennaris A, Barras F, and Collet J-F. Oxidative stress, protein damage and repair in bacteria. *Nat Rev Microbiol.* 2017;15(7):385-96.
33. Smejkal GB, and Kakumanu S. Enzymes and their turnover numbers. *Expert Rev Proteomics.* 2019;16(7):543-4.
34. Iwase T, Tajima A, Sugimoto S, Okuda K-i, Hironaka I, Kamata Y, et al. A simple assay for measuring catalase activity: A visual approach. *Sci Rep.* 2013;3(1):3081.
35. Winterbourn CC. Toxicity of iron and hydrogen peroxide: the Fenton reaction. *Toxicol Lett.* 1995;82-83:969-74.
36. Mitchell RL, and Anderson IC. Catalase Photoinactivation. *Science.* 1965;150(3692):74-.
37. Feierabend J, and Engel S. Photoinactivation of catalase *in vitro* and in leaves. *Arch Biochem Biophys.* 1986;251(2):567-76.
38. Dwyer DJ, Belenky PA, Yang JH, MacDonald IC, Martell JD, Takahashi N, et al. Antibiotics induce redox-related physiological alterations as part of their lethality. *Proc Natl Acad Sci U S A.* 2014;111(20):E2100-E9.
39. Wood BR, Hammer L, Davis L, and McNaughton D. Raman microspectroscopy and imaging provides insights into heme aggregation and denaturation within human erythrocytes. *J Biomed Opt.* 2005;10(1):014005.
40. Liu X, and Kokare C. In: Brahmachari G ed. *Biotechnology of Microbial Enzymes*. Academic Press; 2017:267-98.
41. Bremmer DN, Bauer KA, Pouch SM, Thomas K, Smith D, Goff DA, et al. Correlation of checkerboard synergy testing with time-kill analysis and clinical outcomes of extensively drug-resistant *Acinetobacter baumannii* respiratory infections. *Antimicrobial agents and chemotherapy.* 2016;60(11):6892-5.

42. Asokan GV, Ramadhan T, Ahmed E, and Sanad H. WHO Global Priority Pathogens List: A bibliometric analysis of medline-pubMed for knowledge mobilization to infection prevention and control practices in Bahrain. *Oman Med J.* 2019;34(3):184-93.
43. Howard A, O'Donoghue M, Feeney A, and Sleator RD. *Acinetobacter baumannii*: an emerging opportunistic pathogen. *Virulence.* 2012;3(3):243-50.
44. Bodey GP, Bolivar R, Fainstein V, and Jadeja L. Infections caused by *Pseudomonas aeruginosa*. *Rev Infect Dis.* 1983;5(2):279-313.
45. Kurtz JR, Goggins JA, and McLachlan JB. *Salmonella* infection: Interplay between the bacteria and host immune system. *Immunol Lett.* 2017;190:42-50.
46. Manero A, and Blanch AR. Identification of *Enterococcus spp.* with a biochemical key. *Appl Environ Microbiol.* 1999;65(10):4425-30.
47. Linley E, Denyer SP, McDonnell G, Simons C, and Maillard J-Y. Use of hydrogen peroxide as a biocide: new consideration of its mechanisms of biocidal action. *J Antimicrob Chemother.* 2012;67(7):1589-96.
48. Brown A, Lo D, Sharpe C, and Tong C. Increased intracellular hydrogen peroxide observed in *Escherichia coli* in the presence of two classes of antibiotics. *J Exp Microbiol Immunol.* 2012;16:17-23.
49. Goswami M, Mangoli SH, and Jawali N. Involvement of reactive oxygen species in the action of ciprofloxacin against *Escherichia coli*. *Antimicrob Agents Chemother.* 2006;50(3):949-54.
50. Mulcahy LR, Isabella VM, and Lewis K. *Pseudomonas aeruginosa* biofilms in disease. *Microb Ecol.* 2014;68(1):1-12.
51. Chen H, Wubbolts RW, Haagsman HP, and Veldhuizen EJA. Inhibition and eradication of *Pseudomonas aeruginosa* biofilms by host defence peptides. *Sci Rep.* 2018;8(1):10446.
52. James GA, Swogger E, Wolcott R, Pulcini Ed, Secor P, Sestrich J, et al. Biofilms in chronic wounds. *Wound Repair Regen.* 2008;16(1):37-44.
53. Goeres DM, Loetterle LR, Hamilton MA, Murga R, Kirby DW, and Donlan RM. Statistical assessment of a laboratory method for growing biofilms. *Microbiology.* 2005;151(3):757-62.
54. Peyrusson F, Varet H, Nguyen TK, Legendre R, Sismeiro O, Coppée J-Y, et al. Intracellular *Staphylococcus aureus* persisters upon antibiotic exposure. *Nat Commun.* 2020;11(1):2200.
55. Lehar SM, Pillow T, Xu M, Staben L, Kajihara KK, Vandlen R, et al. Novel antibody–antibiotic conjugate eliminates intracellular *S. aureus*. *Nature.* 2015;527(7578):323-8.
56. Rogers DE. Studies on bacteriemia. I. Mechanisms relating to the persistence of bacteriemia in rabbits following the intravenous injection of staphylococci. *J Exp Med.* 1956;103(6):713-42.
57. Raineri EJM, Altulea D, and van Dijl JM. Staphylococcal trafficking and infection—from 'nose to gut' and back. *FEMS Microbiol Rev.* 2021;46(1).
58. Velasco E, Byington R, Martins CAS, Schirmer M, Dias LMC, and Gonçalves VMSC. Comparative study of clinical characteristics of neutropenic and non-neutropenic adult cancer patients with bloodstream infections. *Eur J Clin Microbiol Infect Dis.* 2006;25(1):1-7.
59. Das D, and Bishayi B. Staphylococcal catalase protects intracellularly survived bacteria by destroying H_2O_2 produced by the murine peritoneal macrophages. *Microb Pathog.* 2009;47(2):57-67.
60. Day WA, Sajecki JL, Pitts TM, and Joens LA. Role of catalase in *Campylobacter jejuni* intracellular survival. *Infect Immun.* 2000;68(11):6337-45.
61. Beavers WN, and Skaar EP. Neutrophil-generated oxidative stress and protein damage in *Staphylococcus aureus*. *Pathog Dis.* 2016;74(6).
62. Guerra FE, Borgogna TR, Patel DM, Sward EW, and Voyich JM. Epic immune battles of history: Neutrophils vs. *Staphylococcus aureus*. *Front Cell Infect Microbiol.* 2017;7(286).
63. Yang X, Shi G, Guo J, Wang C, and He Y. Exosome-encapsulated antibiotic against intracellular infections of methicillin-resistant *Staphylococcus aureus*. *Int J Nanomedicine.* 2018;13:8095-104.
64. Dai T, Kharkwal GB, Tanaka M, Huang Y-Y, Bil de Arce VJ, and Hamblin MR. Animal models of external traumatic wound infections. *Virulence.* 2011;2(4):296-315.

65. Fleming A. On the antibacterial action of cultures of a *Penicillium*, with special reference to their use in the isolation of *B. influenzæ*. *Br J Exp Pathol.* 1929;10(3):226-36.
66. Hutchings MI, Truman AW, and Wilkinson B. Antibiotics: past, present and future. *Curr Opin Microbiol.* 2019;51:72-80.
67. Yadav S, and Kapley A. Antibiotic resistance: Global health crisis and metagenomics. *Biotechnol Rep (Amst).* 2021;29:e00604-e.
68. Mishra S, and Imlay J. Why do bacteria use so many enzymes to scavenge hydrogen peroxide? *Arch Biochem Biophys.* 2012;525(2):145-60.
69. Schwartz CE, Krall J, Norton L, McKay K, Kay D, and Lynch RE. Catalase and superoxide dismutase in *Escherichia coli*. *J Biol Chem.* 1983;258(10):6277-81.
70. Mandell GL. Catalase, superoxide dismutase, and virulence of *Staphylococcus aureus*. *In vitro* and *in vivo* studies with emphasis on staphylococcal--leukocyte interaction. *J Clin Invest.* 1975;55(3):561-6.
71. Park B, Nizet V, and Liu GY. Role of *Staphylococcus aureus* catalase in niche competition against *Streptococcus pneumoniae*. *J Bacteriol.* 2008;190(7):2275-8.
72. Chen G, Qiu H, Prasad PN, and Chen X. Upconversion Nanoparticles: Design, Nanochemistry, and Applications in Theranostics. *Chem Rev.* 2014;114(10):5161-214.
73. Hui J, Li R, Phillips EH, Goergen CJ, Sturek M, and Cheng J-X. Bond-selective photoacoustic imaging by converting molecular vibration into acoustic waves. *Photoacoustics.* 2016;4(1):11-21.
74. Donlan RM, and Costerton JW. Biofilms: survival mechanisms of clinically relevant microorganisms. *Clin Microbiol Rev.* 2002;15(2):167-93.
75. Mascio CTM, Alder JD, and Silverman JA. Bactericidal action of daptomycin against stationary-phase and nondividing *Staphylococcus aureus* cells. *Antimicrob Agents Chemother.* 2007;51(12):4255-60.
76. Keren I, Kaldalu N, Spoering A, Wang Y, and Lewis K. Persister cells and tolerance to antimicrobials. *FEMS Microbiol Lett.* 2004;230(1):13-8.
77. Prapagdee B, Eiamphungporn W, Saenkham P, Mongkolsuk S, and Vattanaviboon P. Analysis of growth phase regulated KatA and CatE and their physiological roles in determining hydrogen peroxide resistance in *Agrobacterium tumefaciens*. *FEMS Microbiol Lett.* 2004;237(2):219-26.
78. Das D, Saha SS, and Bishayi B. Intracellular survival of *Staphylococcus aureus*: correlating production of catalase and superoxide dismutase with levels of inflammatory cytokines. *Inflamm Res.* 2008;57(7):340-9.
79. Liu GY, and Nizet V. Color me bad: microbial pigments as virulence factors. *Trends Microbiol.* 2009;17(9):406-13.
80. Dong P-T, Lin H, Huang K-C, and Cheng J-X. Label-free quantitation of glycated hemoglobin in single red blood cells by transient absorption microscopy and phasor analysis. *Sci Adv.* 2019;5(5):eaav0561.

Figures and legends

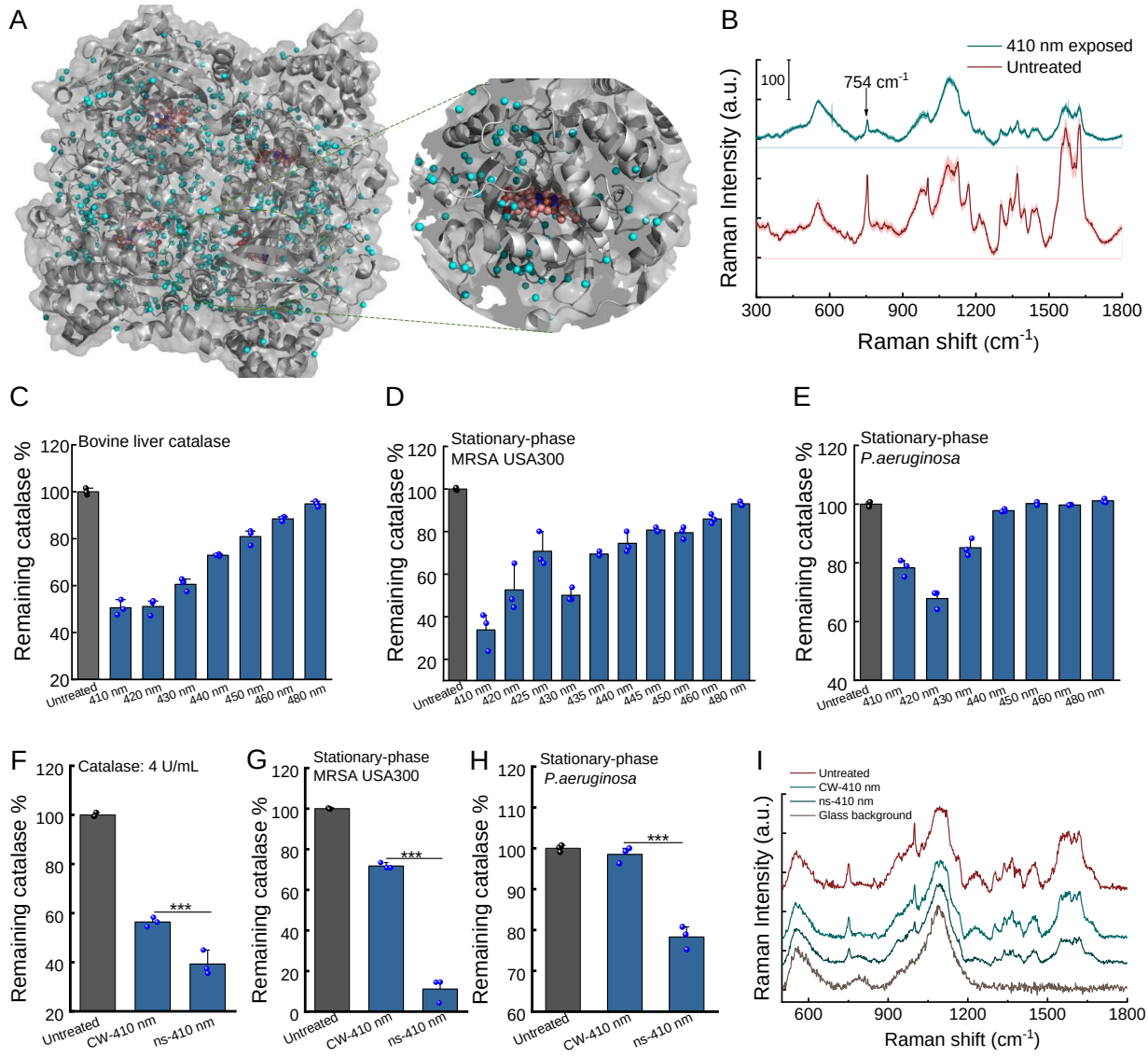

Figure 1. Catalase inactivation by continuous-wave (CW) and pulsed blue light in a wavelength dependent manner. **A**. *P. aeruginosa* catalase structure through PyMOL simulation. PDB 4E37. **B**. Raman spectra of a bovine liver catalase film dried on a cover slide before (untreated) and after 410 nm light exposure. The Raman peak at 754 cm^{-1} was highlighted by an arrow. 410 nm: 50 mW/cm^2, 10 min. Standard deviations at each Raman shift were shown in shadow. **C**-**E**. Remaining catalase percent of bovine liver catalase (**C**, 2.5 U/ml), stationary-phase MRSA USA300 (**D**) and stationary-phase *P. aeruginosa* PAO1 (**E**) under blue light exposure at different wavelengths. **F**-**H**. Comparison of CW and ns-410 nm exposure on inhibiting bovine liver catalase (**F**, 4 U/ml), catalase from stationary-phase MRSA USA300 (**G**) and stationary-phase *P. aeruginosa* PAO1 (**H**). **I**. Raman spectra of bovine liver catalase film dried on a cover slide under CW-410 and ns-410 exposure. Light: 50 mW/cm^2, 5 min. Data: Mean+SD from three replicates for panels **B**-**H**. Statistical analysis was obtained through student's unpaired *t*-test. ***: $p<0.001$.

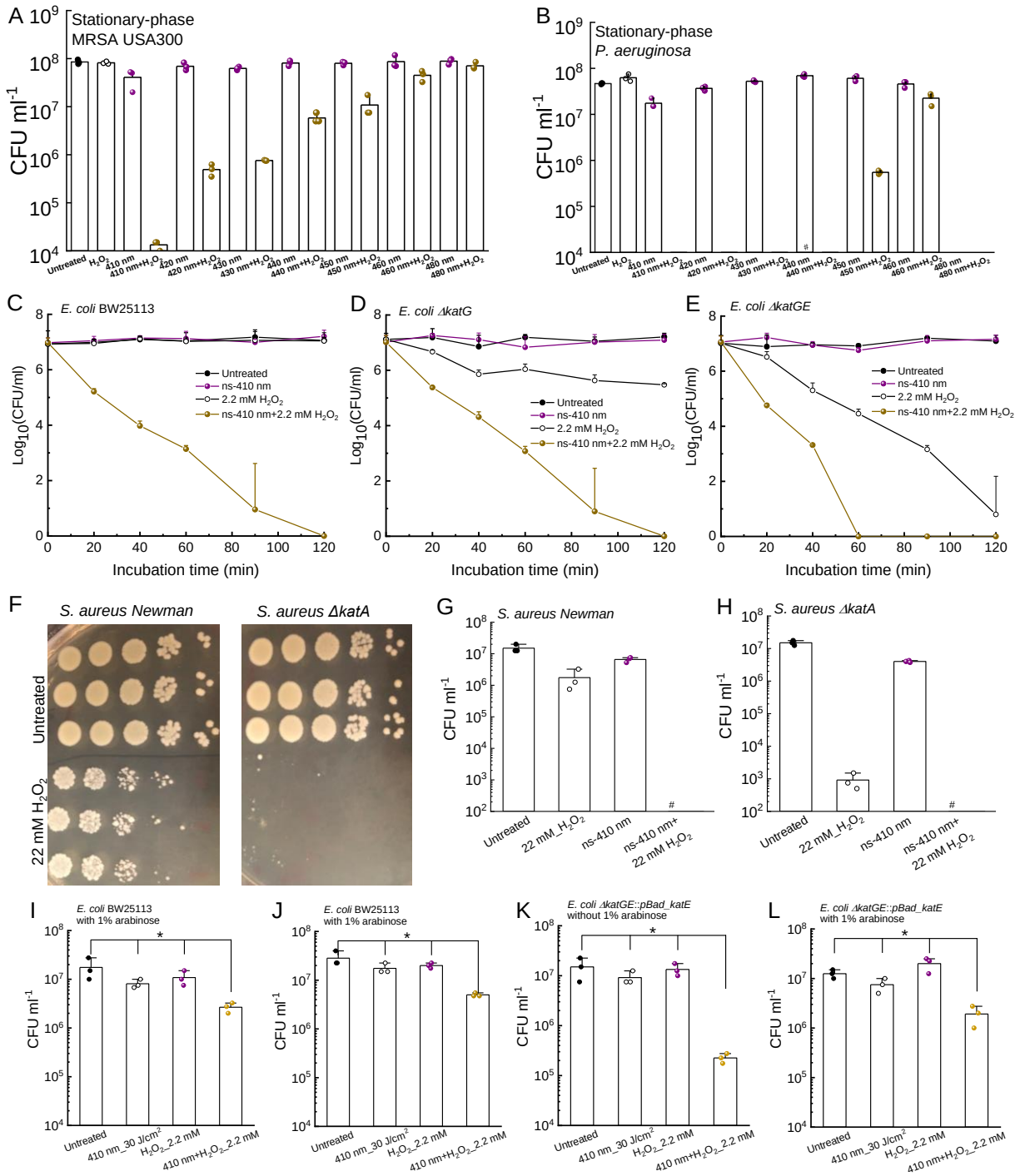

Figure 2. Photoinactivation of catalase effectively sensitizes pathogenic bacteria to H_2O_2. A. CFU ml^{-1} of stationary-phase MRSA USA300 under various treatments. Dose: 50 mW/cm^2, 5 min. H_2O_2: 22 mM, 30-min incubation time. **B**. CFU ml^{-1} of stationary-phase *P. aeruginosa* PAO1 under various treatments. Dose: 50 mW/cm^2, 5 min. H_2O_2: 22 mM, 30-min incubation time. **C-E**. Time-killing curves of wild type *E. coli* BW25113 (**C**), *E. coli ΔkatG* (**D**), *E. coli ΔkatGE* (**E**) under different treatment schemes. ns-410 nm: 30 mW, 8 min, 14 J/cm^2. **F**. CFU plates of *S. aureus Newman* along with its isogenic catalase mutant *S. aureus ΔkatA* with/without H_2O_2 treatment. **G-H.** CFU ml^{-1} of *S. aureus Newman* (**G**) and *S. aureus ΔkatA*

(**H**) under different treatment schemes. **I**-**L**: Viable *E. coli* BW25113 (**I**-**J**) and *E. coli ΔkatGE*::*pBad_katE* (**K**-**L**) were enumerated after incubating with/without H_2O_2 (2.2 mM) for 30 min in the absence/presence of arabinose (4 hours) after 30-J/cm^2 410 nm treatment. Data: Mean+SD from at least three biological replicates for all panels. Pound sign (#) indicates the CFU results are below the detection limit. Statistical analysis was obtained by student unpaired *t*-test (compared to the untreated group) and one-way ANOVA. ***: $p<0.001$; *: $p<0.05$.

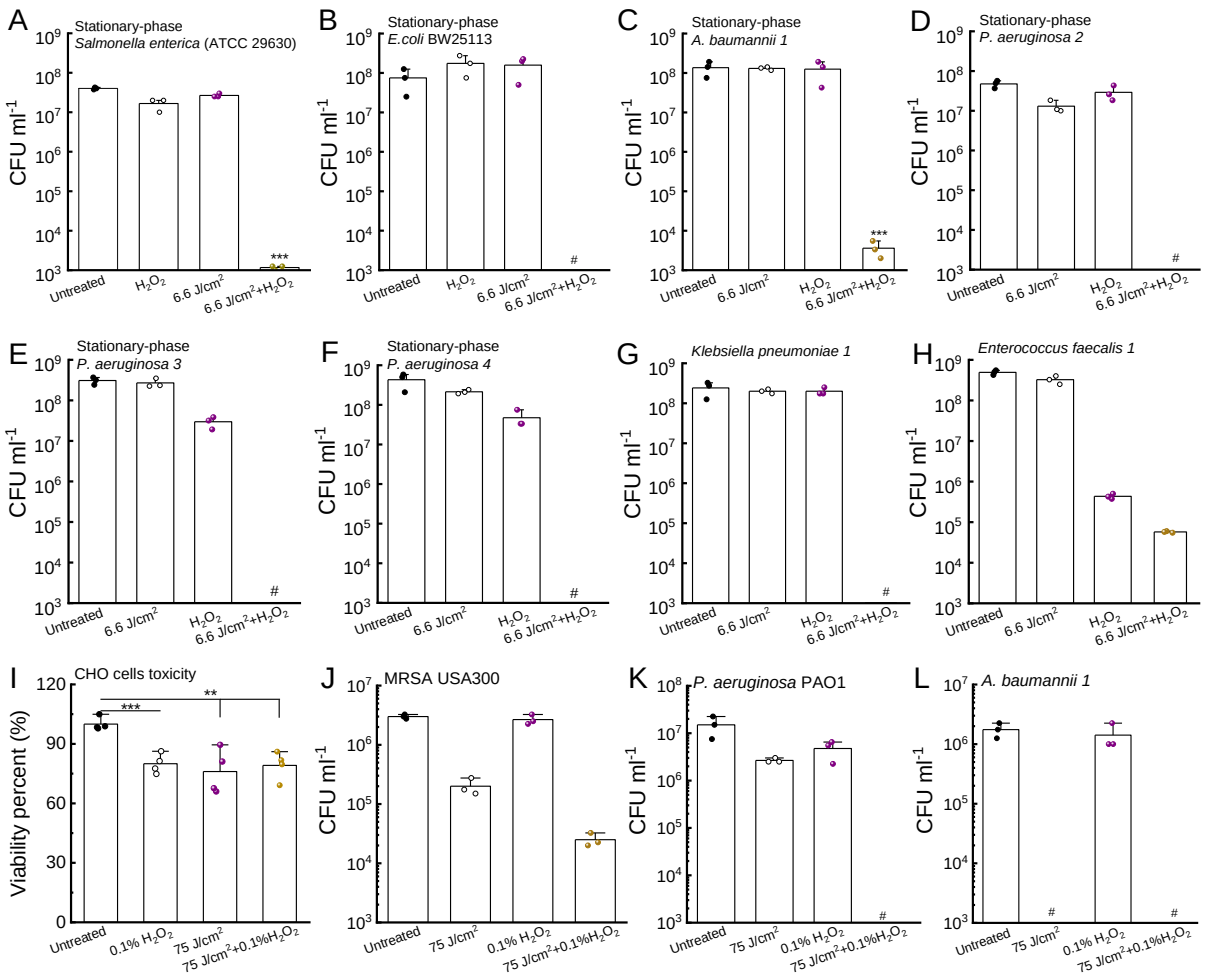

Figure 3. Photoinactivation of catalase sensitizes wide-ranging pathogenic bacteria to H_2O_2. A-H. CFU ml^{-1} of stationary-phase *Salmonella enterica* ATCC 29630 (**A**), stationary-phase *E. coli* BW25113 (**B**), stationary-phase *A. baumannii 1* (**C**), stationary-phase *P. aeruginosa* strains (**D-F**), *Klebsiella pneumonia 1* (**G**), *Enterococcus faecalis 1* (**H**) under various treatment schemes. 410 nm exposure: 6.6 J/cm^2, H_2O_2: 22 mM, 30-min culture time (for **A-H**). **I**. Toxicity test of CHO cells by MTT assay under different treatment schemes. **J-L**. CFU ml^{-1} of log-phase MRSA USA300 (**J**), log-phase *P. aeruginosa* PAO1 (**K**), and log-phase *A. baumannii 1* (**L**) under different treatment schemes. 410 nm exposure: 75 J/cm^2, H_2O_2: 0.1%. Serial dilution or MTT assay was conducted after 1-min incubation time (for **I-L)**. Data: Mean+SD from three replicates for all panels. Pound sign (#) indicates the CFU results are below the detection limit. Significant difference was determined by student's unpaired *t*-test and one-way ANOVA. Significant from all the other groups unless notified. ***: $p<0.001$.

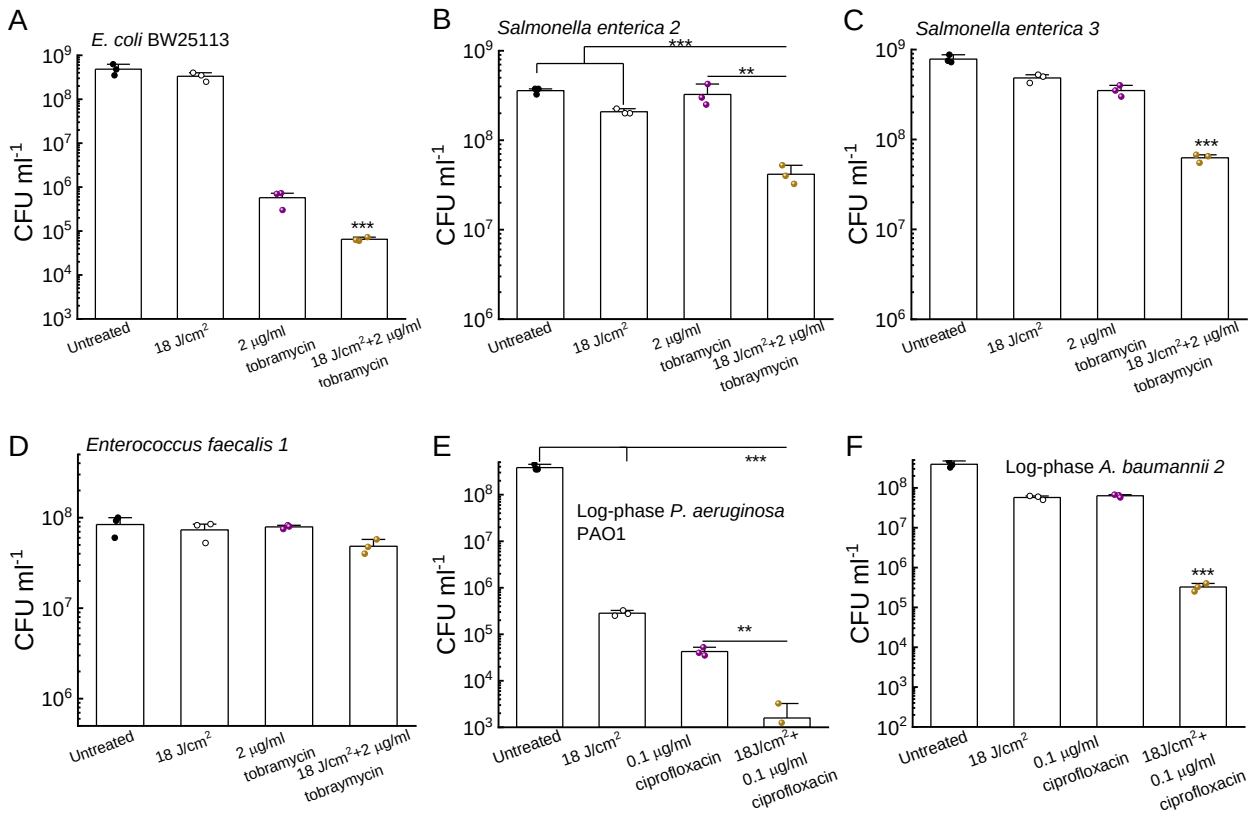

Figure 4. Photoinactivation of catalase sensitizes pathogenic bacteria to certain antibiotics. **A**. CFU ml^{-1} of *E. coli* BW25113 under different treatments. **B-C**. CFU ml^{-1} of *Salmonella enterica* under different treatments. CFU enumeration was obtained by incubation with tobramycin in TSB for 4 hours. **D**. CFU ml^{-1} of *Enterococcus faecalis 1* under the same treatments as in **B-C**. **E-F**. CFU ml^{-1} of log-phase *P. aeruginosa* PAO1 (**E**) along with *A. baumannii 2* under different treatment schemes. CFU enumeration was achieved after incubation with ciprofloxacin in TSB for 4 hours. Data: Mean+SD from three replicates for all the panels. Statistical analysis was determined by student's unpaired *t*-test and one-way ANOVA. ***: $p<0.001$, **: $p<0.01$. Significant from other groups unless notified.

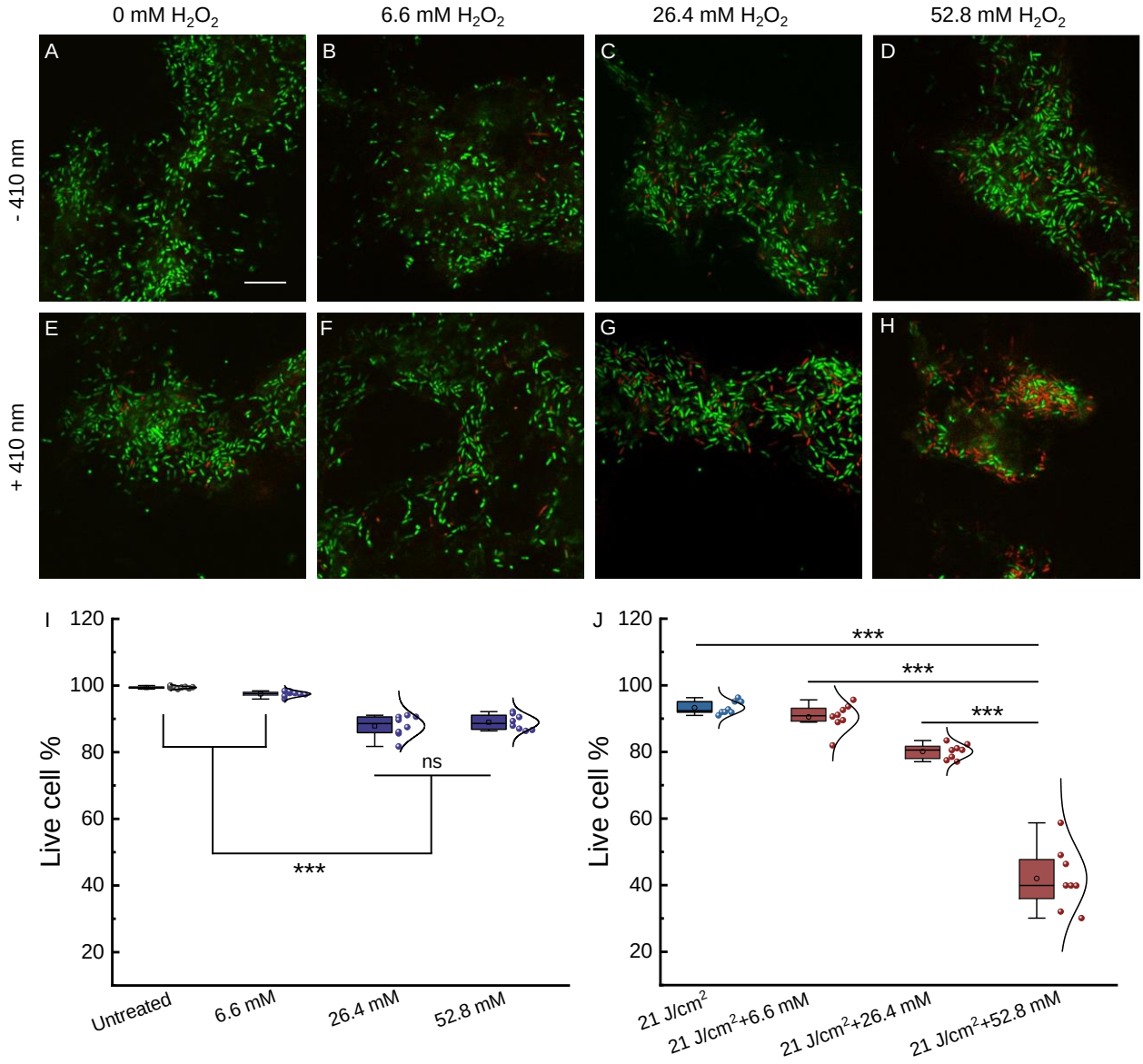

Figure 5. Confocal laser scanning microscopy of live/dead bacteria inside *P. aeruginosa* PAO1 biofilms after different treatments. A-D. Merged live/dead *P. aeruginosa* biofilms with various H_2O_2 treatments. **E-H**. Merged live/dead *P. aeruginosa* biofilms after 410 nm exposure combined with various H_2O_2 treatments. **I-J**. Quantitative analysis of the live cell percent of *P. aeruginosa* biofilms among the above eight groups. Live cell percent was calculated from eight different field of views. Box- and whisker-plots: mean, circle; median, horizontal line; box range, perc 25, 75. Scalar bar=10 µm. Live: SYTO 9. Dead: PI. 410 nm laser: ns-410 nm, 35 mW, 10 min. H_2O_2: 30-min incubation time. Statistical analysis was determined through student's unpaired *t*-test and one-way ANOVA. ***: $p<0.001$, ns: not significant.

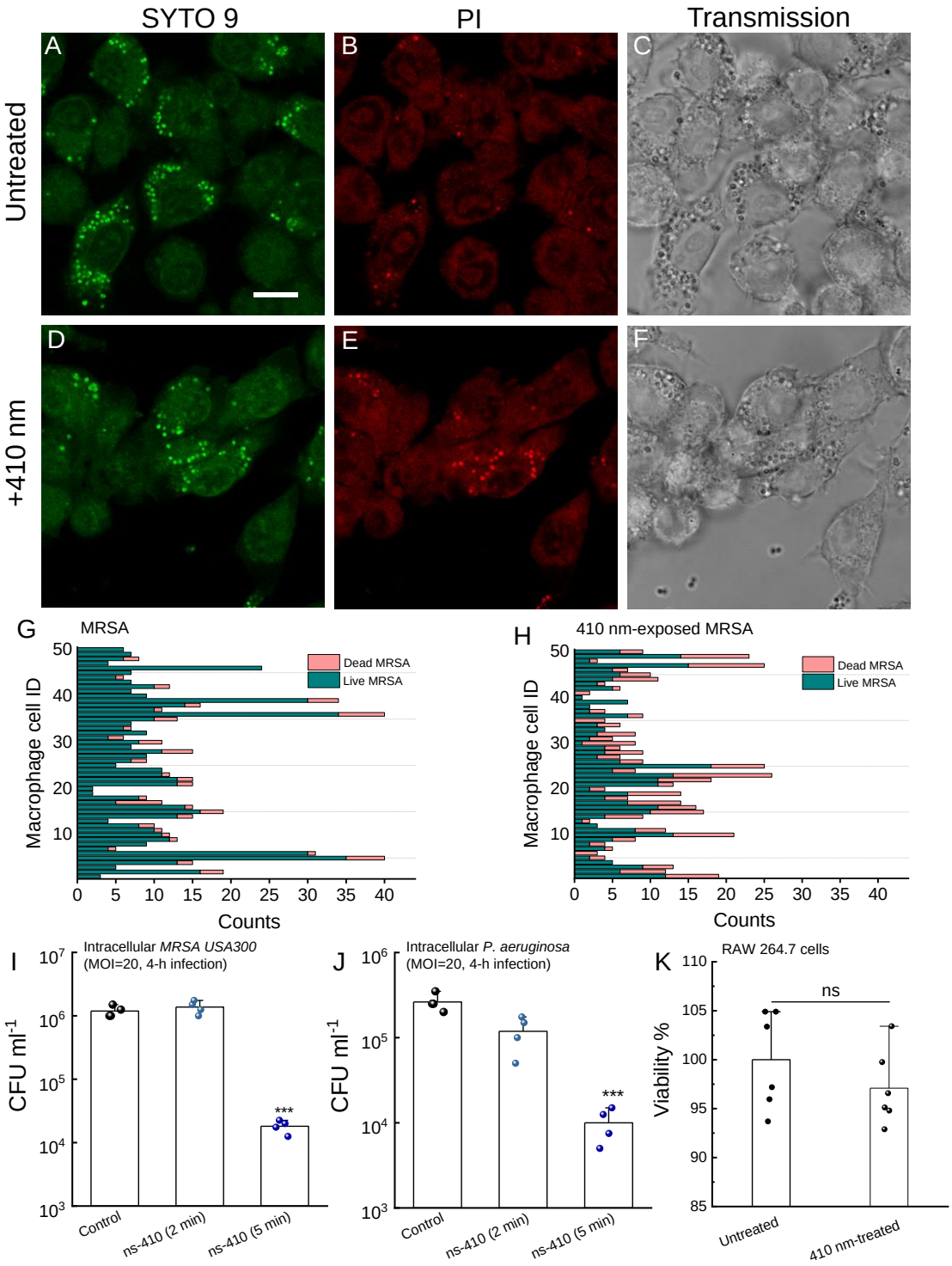

Figure 6. Photoinactivation of catalase assists macrophages to eliminate intracellular bacteria. **A-C**. Confocal images of live (SYTO 9, **A**), dead (PI, **B**) and corresponding transmission images (**C**) of intracellular MRSA USA300 inside RAW 264.7 macrophages after MRSA USA300 infected RAW 264.6 cells for 1 h at a multiplicity of infection (MOI) of 100 in serum-free DMEM media. **D-F**. Confocal images of live (SYTO 9, **D**), dead (PI, **E**) and corresponding transmission images (**F**) of intracellular MRSA USA300 inside RAW 264.7 macrophages after 410 nm-exposed MRSA USA300 infected RAW 264.7 cells

for 1 h at a MOI of 100. 410 nm: 35 mW/cm^2, 8 min. **G**-**H**. Quantitative analysis of the amount of live/dead MRSA inside single RAW 264.7 cells from the above two scenarios. Imaging result was a representative of two biological repeats. **I**. CFU ml^{-1} of intracellular MRSA USA300 after MRSA (with/without 410 nm exposure) infected RAW 264.7 cells for 4 hours at a MOI of 20. **J**. CFU ml^{-1} of intracellular *P. aeruginosa* after *P. aeruginosa* PAO1 (with/without 410 nm exposure) infected RAW 264.7 cells for 4 hours at a MOI of 20. **K**. Survival percent of uninfected RAW 264.7 cells with/without 410 nm exposure. 410 nm: 50 mW/cm^2. Data: Mean+SD from three replicates for panels **I**-**K**. Significant difference was determined by One-way ANOVA (significant from other two groups). ***: $p<0.001$, **: $p<0.01$, ns: not significant.

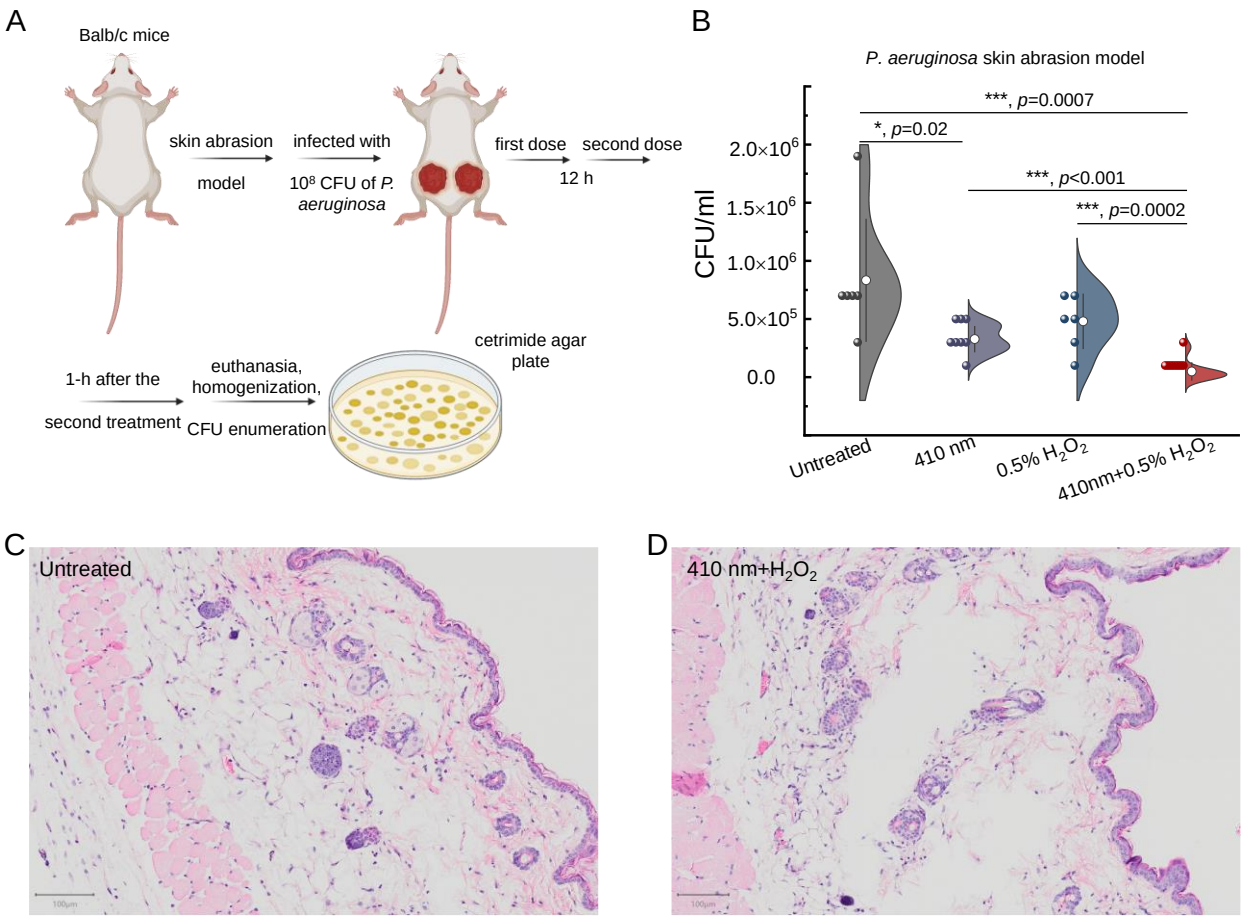

Figure 7. Photoinactivation of catalase reduces *P. aeruginosa* burden in a *P. aeruginosa*-induced mouse skin abrasion model. **A**. Schematic illustration of *in vivo* mice experiment. **B**. CFU ml^{-1} of *P. aeruginosa* PAO1 from the infected wound tissues among four different groups. **C**-**D**. Histology analysis of mice skin from untreated group along with 410 nm plus H_2O_2 treated group. Scalar bar=100 μm. Data: Mean±SD from at least six replicates (N=3-4 mice/group, 6-8 infected area/group). 410 nm: 120 J/cm^2. H_2O_2: 0.5%. Significant difference was determined by student's unpaired *t*-test and one-way ANOVA. ***: $p<0.001$, **: $p<0.01$, *: $p<0.05$, ns: not significant. An outlier was removed based on the Dixon's Q test and whisker box plot.